Lattice investigation of custodial two-Higgs-doublet model at weak quartic couplings

Guilherme Catumba[a,b], **Atsuki Hiraguchi**[c,d], **Wei-Shu Hou**[e], **Karl Jansen**[f], **Ying-Jer Kao**[e,g], **C.-J. David Lin**[c,h], **Alberto Ramos**[b], **Mugdha Sarkar**[c,e]

[a] *Department of Physics, University of Milano-Bicocca & INFN Milano–Bicocca, Piazza della Scienza 3, 20126, Milano, Italy*
[b] *Instituto de Fisica Corpuscular (IFIC), CSIC-Universitat de Valencia, 46071, Valencia, Spain*
[c] *Institute of Physics, National Yang Ming Chiao Tung University, Hsinchu 30010, Taiwan*
[d] *CCSE, Japan Atomic Energy Agency, 178-4-4, Wakashiba, Kashiwa, Chiba 277-0871, Japan*
[e] *Department of Physics, National Taiwan University, Taipei 10617, Taiwan*
[f] *Deutsches Elektronen-Synchrotron DESY, Platanenallee 6, 15738 Zeuthen, Germany*
[g] *Centre for Theoretical Physics and Centre for Quantum Science and Technology, National Taiwan University, Taipei 10607, Taiwan*
[h] *Centre for High Energy Physics, Chung-Yuan Christian University, Taoyuan 32023, Taiwan*

Abstract

The $SU(2)-$gauged custodial two-Higgs-doublet model, which shares the same global-symmetry properties with the standard model, is studied non-perturbatively on the lattice. The additional Higgs doublet enlarges the scalar spectrum and opens the possibility for spontaneous breaking of the global symmetry. In this work we start by showing the occurrence of spontaneous breaking of the custodial symmetry in a region of the parameter space of the model. Following this, both the spectrum and the running of the gauge coupling of are examined at weak quartic couplings in the presence of the custodial symmetry. The calculations are performed with energy cutoffs ranging from 300 to 600 GeV on a line of constant standard model physics, obtained by tuning bare couplings to fix the ratio between the masses of the Higgs and the W bosons, as well as the value of the renormalized gauge coupling at the scale of the W boson mass. The realizable masses for the additional scalar states are explored. For the choice of bare quartic couplings in this work, the estimated lower bound of these masses is found to be well below the W boson mass, and independent of the cutoff. We also study the finite temperature electroweak transition along this line of constant standard model physics, revealing properties of a smooth crossover behavior.

CONTENTS

I. INTRODUCTION

The standard model (SM) has been very successful in describing experimental results at the Large Hadron Collider (LHC) and other facilities. Nevertheless, physics beyond the SM (BSM) is needed in order to account for many phenomena. For instance, there are no dark-matter candidates in the theory. Another prominent problem is the lack of explanation for the excess of matter over antimatter in the universe. As suggested by Sakharov [1], to explain electroweak baryogenesis CP violation and a strong first-order electroweak phase transition (EWPT) is needed. The amount of CP violation present in the SM is not enough for this purpose. In addition, it is well established that the SM does not contain a first-order electroweak phase transition at the measured Higgs boson mass, $m_h \approx 125$ GeV [2–6]. Such issues have been driving the search for BSM physics.

One natural scenario of BSM physics is the existence of extra scalar fields. While the Higgs sector of the SM is the minimal structure for realising electroweak symmetry breaking, there are no compelling reasons for the absence of additional Higgs doublets. Indeed, a structure analogous to fermion families can be introduced in the scalar sector. Such an extension of the SM can, arguably, result in enough CP violation, and it can also alter the character of the electroweak phase transition. These features motivate the search of BSM Higgs doublets. Taking into account the phenomenological constraints imposed by the measurement of the ρ parameter [7], a viable and simple extension of the SM is the addition of a second $SU(2)$ doublet of scalar fields. This is known as the two-Higgs-doublet model (2HDM).

In the continuum, we denote the fields of the two scalar doublets by $(i = 1, 2)$

$$\Phi_i^c = \begin{pmatrix} \phi_i^1 + i\phi_i^2 \\ \\ \phi_i^3 + i\phi_i^4 \end{pmatrix} . \tag{1}$$

The Lagrangian of the 2HDM, coupled to $SU(2)$ gauge fields is

$$\mathcal{L} = \sum_{i=1}^{2} \left(D_\mu \Phi_n^c\right)^\dagger \left(D^\mu \Phi_n^c\right) - \frac{1}{4} G_{\mu\nu}^a G^{a,\mu\nu} - V_{\text{2HDM}}(\Phi_1^c, \Phi_2^c) \,, \tag{2}$$

where $D_\mu = \partial_\mu - igA_\mu^a \sigma^a/2$ is the covariant derivative, with A_μ^a the real components of the $SU(2)$ algebra-valued gauge field, σ^a the Pauli matrices, g the gauge coupling constant, and $G_{\mu\nu}^a = \partial_\mu A_\nu^a - \partial_\nu A_\mu^a + g\varepsilon^{abc} A_\mu^b A_\nu^c$ the field strength tensor. The most general gauge-invariant scalar potential, $V_{\text{2HDM}}(\Phi_1^c, \Phi_2^c)$, can be written in terms of the products $\Phi_i^{c,\dagger}\Phi_j^c$, $i, j = 1, 2$. Since we are interested in the lattice application, we consider from now on the case of real couplings only. This is the CP-conserving 2HDM [8, 9]. With this choice, the most general renormalizable scalar potential of the 2HDM has 10 real parameters, and reads

$$\begin{aligned} V_{\text{2HDM}} = {} & \mu_{11}^2 \Phi_1^{c,\dagger}\Phi_1^c + \mu_{22}^2 \Phi_2^{c,\dagger}\Phi_2^c + \mu_{12}^2 \,\text{Re}(\Phi_1^{c,\dagger}\Phi_2^c) + \lambda_1 (\Phi_1^{c,\dagger}\Phi_1^c)^2 + \lambda_2 (\Phi_2^{c,\dagger}\Phi_2^c) \\ & + \lambda_3 (\Phi_1^{c,\dagger}\Phi_1^c)(\Phi_2^{c,\dagger}\Phi_2^c) + \lambda_4 (\Phi_1^{c,\dagger}\Phi_2^c)(\Phi_2^{c,\dagger}\Phi_1^c) + \lambda_5 \,\text{Re}(\Phi_1^{c,\dagger}\Phi_2^c)^2 \\ & + \text{Re}(\Phi_1^{c,\dagger}\Phi_2^c) \left[\lambda_6 (\Phi_1^{c,\dagger}\Phi_1^c) + \lambda_7 (\Phi_2^{c,\dagger}\Phi_2^c)\right] . \end{aligned} \tag{3}$$

The above model yields an enlarged spectrum compared to the SM Higgs sector. Its details depend crucially on the region of the parameter space. In the perturbative treatment of the $SU(2)-$gauged scalar theory with the potential in eq. (3), the relevant parameter regions are those with the Higgs mechanism active, where the spectrum is expected to contain five scalar states, $h, H, A, H^\pm$. In the Higgs-basis, where only one of the fields acquires a vacuum expectation value, v —ϕ_2 in the case at hand—, the analysis of the mass matrices reveals the following tree-level relations [10],

$$m_{H^\pm}^2 = \mu_{11}^2 + \frac{1}{2}\lambda_3 v^2 \,, \tag{4}$$

$$m_A^2 = m_{H^\pm}^2 + \frac{1}{2}[\lambda_4 - \lambda_5] v^2 \,, \tag{5}$$

$$\mathcal{M} = v^2 \begin{pmatrix} \mu_{22}^2/v^2 & \lambda_6 \\ \lambda_6 & \mu_{11}^2/v^2 + \frac{1}{2}[\lambda_3 + \lambda_4 + \lambda_5] \end{pmatrix} . \tag{6}$$

The 'charged' scalar states labelled by $H^{\pm}$ and the pseudo-scalar state, A, have well defined masses. On the other hand, the remaining two CP-even scalars require the diagonalization of $\mathcal{M}$. However, in the $\mathbb{Z}_2$-symmetric limit with $\mu_{12} = \lambda_6 = \lambda_7 = 0$, it is straightforward to obtain $m_h^2 = v^2\mu_{22}^2$ and $m_H^2 = \mu_{11}^2/v^2 + \frac{1}{2}[\lambda_3 + \lambda_4 + \lambda_5]$.

Other than the enlarged spectrum, this extension can have a rich phenomenology, including, as we have mentioned, extra CP violation and possibly a first order electroweak phase transition. Additionally, these models can also have other phenomenological applications. In the class of models discussed in refs. [11–13] the extra states in the spectrum are used as dark matter candidates, and are modeled to not interact with the quarks and leptons.

While the augmented parameter space of the extended theory is a desirable feature due to the rich phenomenology it can provide, the parameters of the potential cannot be chosen in a completely arbitrary way since, for instance, there are requirements of stability and boundedness of the potential [14, 15]. Furthermore, any proposed 2HDM model should comply with current experimental evidence for SM quantities. In particular, it should suppress the flavour-changing neutral current (FCNC) processes, as constrained by experiments. On the other hand, various studies have shown that the phenomenology of the theory is dictated by the symmetries of the scalar potential [16–20], particularly, in ref. [21] the symmetries were related to physical parameters. One of the earliest symmetry-related proposals [22, 23] to eliminate tree-level FCNC takes the Lagrangian to be $\mathbb{Z}_2$-symmetric under the change of sign of one of the scalar doublets. In ref. [24], however, it was claimed that the $\mathbb{Z}_2$-symmetry may not be required to suppress the FCNC processes, if certain mass-mixing hierarchies are found in the fermion flavour sector, with an additional alignment of the CP-even Higgs mass eigenstates [25]. This in turn may correspond to $\mathcal{O}(1)$ quartic couplings, that are also thought to be required for a first-order electroweak phase transition [26].

The amount of literature on the 2HDM is vast and ongoing (a general review can be found in ref. [27]). There are analyses of the parameter space, stability and boundedness of the potential [14, 15, 28], phenomenological implications [16–20], and group theoretical aspect of the global symmetries [21]. Most of these studies are performed at tree-level, and while the scalar sector of the SM is weakly coupled, recent investigations suggest that large scalar-field quartic couplings in the BSM sector may be needed to have a strong first order EWPT [26, 29–31]. The large values of quartic coupling in itself puts in doubt the perturbative approach to consider these questions (cf. [32]). Moreover, scalar field theories are expected to be trivial [33–37]. They must be understood as effective theories, only valid in the weakly coupled regime. In summary, the large quadratic couplings needed in many phenomenological models and the triviality of scalar field theories requires a study beyond perturbation theory.

Lattice techniques allow a fully non-perturbative study of scalar models. In this work we consider a simplified version of the Higgs theories without the photon and the fermions, namely a $SU(2)$-Higgs model. This theory describes the interaction of the two complex doublets in the fundamental representation with the $SU(2)$ gauge fields. Unlike perturbative investigations, there have not been many lattice studies of 2HDM. In refs. [38, 39] the phase structure and the presence of spontaneous symmetry breaking on the 2HDM was studied, while [40] presented exploratory results on the running of the gauge coupling in different sectors of the parameter space. Furthermore, among other BSM theories, the case of the addition of an extra singlet to the Lagrangian has been explored also on the lattice [41]. Nevertheless, there has not been any lattice computation for the spectrum of the 2HDM. Additionally, the only existing finite temperature investigations of the model were carried out using a 3-dimensional effective field theory [32, 42]. In this work we tackle both of these questions in the weakly coupled 2HDM in four dimensions. Our calculaion is the first lattice study of the 2HDM on a line of constant SM physics. This line is obtained by tuning the bare couplings to reproduce the physical values of the ratio between the SM Higgs and the W boson masses, m_h/m_W, as well as the renormalized gauge coupling at the scale of m_W. We investigate the BSM scalar spectrum and the finite temperature transition at different values of the lattice spacing, corresponding to the cutoff scale in the range of 300 to 600 GeV. We also examine the pattern of spontaneous breaking of the global symmetries. Similar to the finding from the lattice study of the $SU(2) \times SU(2)$-symmetric 2HDM in ref. [39], we confirm the occurrence of the spontaneous breaking of the custodial $SU(2)$ symmetry in 2HDM.

Although the calculation described in this paper is carried out at weak quartic couplings, it is an important first step of our lattice exploration of 2HDM. In particular, it sets the ground for future work at large renormalized quartic couplings on lines of constant SM physics, which are highly relevant to the phenomenology of strong first-order EWPT. The preliminary results of this work can be found in our contributions to the annual conferences on lattice field theory [43–45].

II. STANDARD MODEL PHYSICS WITHIN THE LATTICE 2HDM

One of the main objectives of this work is to build a line of constant standard model physics within the lattice 2HDM at various values of lattice spacing, corresponding to different momentum cutoffs. In order to do so we need to understand the phase structure of the model, namely, the regions of parameter space where the theory is in the Higgs phase, and where and whether spontaneous breaking of the global symmetries occurs.

In the following we introduce the lattice model, summarize the predictions about the phase structure, and outline the strategy for tuning a line of constant SM physics.

A. Lattice Formulation

It is convenient to employ the quaternion formalism for lattice simulations of scalar fields in the fundamental representation. In this approach, the two scalar doublets are represented by 2×2 matrices ($i = 1, 2$),

$$\Phi_i(x) = \sum_{\alpha=1}^{4} \theta_\alpha \hat{\phi}_i^\alpha(x)\,, \tag{7}$$

where $\theta^4 = \frac{1}{2}\mathbb{1}_{2\times2}$ and $\theta^k = \frac{i}{2}\sigma^k$ for $k = 1, 2, 3$ with σ^k being the Pauli matrices. The real scalar fields on the lattice are related to those in eq. (1) through (a is the lattice spacing)

$$\hat{\phi}_i^\alpha = \frac{a}{\sqrt{\kappa_i}}\phi_i^\alpha\,, \tag{8}$$

with κ_i related to the couplings in the continuum 2HDM potential in eq. (3) through

$$a^2\mu_{ii}^2 = \frac{1 - 8\kappa_i - \lambda_i\kappa_i^2}{\kappa_i}\,. \tag{9}$$

While the symmetry structure of the single Higgs model is simple[1], the global symmetries of the 2HDM can be more complicated due to the enlarged parameter space. In order to understand the latter, it is worth starting from the simplest non-interacting scalar theory without gauge fields. This model is invariant under two independent $O(4)$ transformations, one for each Higgs doublet. Since $O(4) \sim SU(2) \times SU(2)$, when gauging the theory, two of the $SU(2)$ (one from each $O(4)$) are identified with each other. After this step there remains a local gauge symmetry, $SU(2)_L$, and two independent global $SU(2)$ symmetries. that the scalar fields Φ_i are in the fundamental representation of $O(4) \sim SU(2) \times SU(2)$, of which one of the subgroups is gauged, $SU(2)_L$, while the other remains as a global symmetry of the theory. This local and global symmetry structure is well understood in the matrix formulation, since the fields Φ_i transform under the $SU(2)_L$ gauge group by a left multiplication, and under the global $SU(2)$ by right multiplication, $\Phi_i \to L(x)\Phi_i R_i$, where both $L(x)$ and R_i belong to the fundamental representations of $SU(2)_L$ and $SU(2)$, respectively. While gauge symmetry forces both $SU(2)_L$ subgroups to be the same, the remaining global symmetry structure depends on the choice of terms in the action.

Previous lattice studies [38–40] have considered an enlarged global symmetry, namely $SU(2) \times SU(2)$, where both scalars can be transformed independently, $R_1 \neq R_2$. In this work we take the $\mathbb{Z}_2$-breaking terms in eq. (3) to vanish, $\mu_{12} = \lambda_6 = \lambda_7 = 0$, defining the so-called inert models. Moreover, by imposing the condition $\lambda_4 = \lambda_5$ we obtain the custodial limit of the 2HDM, where the model shares the same global symmetry with the SM. That is, its action is invariant under global custodial $SU(2)$ transformations where both scalar doublets transform simultaneously and identically, $R_1 = R_2$.

Contrary to the single Higgs case, where no spontaneous symmetry breaking can occur (the gauge symmetry, including its global part, as well as the custodial $SU(2)$ are never broken), the enlarged parameter space of the 2HDM allows

[1] In the scalar sector of the SM, the scalar potential is invariant under a single $O(4) \simeq SU(2) \times SU(2)$. Part of this group is gauged, with the remaining $SU(2)$ being the only global custodial symmetry.

for the breaking of the global symmetries. In this work we study the occurrence of spontaneous symmetry breaking of the custodial symmetry in the 2HDM. This study is relevant for characterizing the different regions of the parameter space, and in particular for finding which of these are suitable for reproducing low energy SM physics.

The lattice action for the custodial 2HDM used in this work can then be written as ($U_\mu(x)$ is the link variable that is an element of the $SU(2)$ gauge group)

$$S_{\text{2HDM}} = \sum_x \Bigg[\sum_{i=1}^{2} \Bigg\{ \sum_{\mu=1}^{4} -2\kappa_i \operatorname{Tr}\left(\Phi_i^\dagger U_\mu \Phi_i(x+\hat{\mu})\right) + \operatorname{Tr}\left(\Phi_i^\dagger \Phi_i\right) + \eta_i \left[\operatorname{Tr}\left(\Phi_i^\dagger \Phi_i\right) - 1\right]^2 \Bigg\} + \eta_3 \operatorname{Tr}\left(\Phi_1^\dagger \Phi_1\right) \operatorname{Tr}\left(\Phi_2^\dagger \Phi_2\right) + 2\eta_4 \operatorname{Tr}\left(\Phi_1^\dagger \Phi_2\right)^2 \Bigg] + S_{\text{YM}}\,, \tag{10}$$

where fields without argument are evaluated at the lattice point x, and S_{YM} is the standard Wilson plaquette action

$$S_{\text{YM}} = \beta \sum_x \sum_{\mu>\nu} \left[1 - \frac{1}{2} \operatorname{Re}\operatorname{Tr} U_{\mu\nu}(x)\right]\,, \tag{11}$$

with $U_{\mu\nu}$ the plaquette on the (μ,ν) plane and $\beta = 4/g^2$. The bare lattice quartic couplings in eq. (10) are related to their continuum counterparts by

$$\begin{aligned} \eta_i &= \lambda_i \kappa_i^2 \text{ for } i = 1,2\,, \\ \eta_i &= \lambda_i \kappa_1 \kappa_2 \text{ for } i = 3,4,5\,. \end{aligned} \tag{12}$$

For the numerical simulations, the scalar and gauge field configurations were generated using the Hybrid Monte Carlo (HMC) algorithm (details in section A). The code implementation for NVIDIA GPUs in the Julia programming language can be found in [46] (documentation can be found in [47]). All error analysis were done using the Γ-method [48], using the free implementation available in [49] (see also [50]).

B. Phase structure, Order Parameters & Symmetry breaking

While the single-Higgs-doublet model, governed by three bare couplings, has a simple phase structure[2], the enlarged parameter space of the 2HDM, as well as the additional symmetries of the system, give rise to a more complicated structure.

In the case of the inert models, it is possible to divide the parameter space in four different regions where none, one, or both scalar doublets are in the Higgs phase [27]. In the perturbative formulation, using the vacuum expectation values, v_i, for each Higgs field this corresponds to:

$$\begin{aligned} &(H_0) : v_1 = v_2 = 0, \\ &(H_2) : v_1 = 0, v_2 \neq 0, \\ &(H_1) : v_1 \neq 0, v_2 = 0, \\ &(H_{12}) : v_1 \neq 0, v_2 \neq 0 \end{aligned} \tag{13}$$

These sectors divide the κ_1, κ_2 plane into four sectors defined by the critical values, κ_i^c.[3] Note, however, that not all four can be seen as separate phases since some of these transitions are crossovers for certain regimes of the couplings. The global symmetries, predicted particle content, and qualitative aspects of each of the phases are summarized in fig. 1. The tree-level bounds for these regions are defined in ref. [51], and in refs. [38, 39] these sectors were studied for the $SU(2) \times SU(2)$-symmetric inert potential non-perturbatively on the lattice.

---

[2] In fact, only a single phase exists in the Higgs-gauge theory. The confinement and Higgs sectors are analytically connected.
[3] Notice that the value of κ_i^c depends on the remaining couplings of the theory.

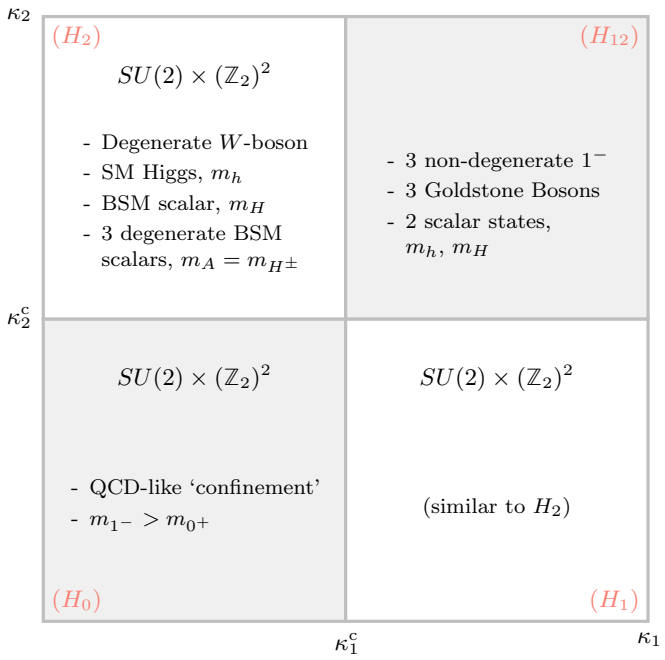

FIG. 1. Summary of the cutodial 2HDM parameter space with the global symmetries and spectrum content for each of the sectors H_0, H_1, H_2, H_{12}. 1^-, and 0^+ represent a vector and a scalar state, respectively.

Sectors (H_1), (H_2), and (H_{12}) have the Higgs mechanism (or the Frohlich-Morchio-Strocchi (FMS) mechanism [52, 53]) active. However, as will be shown in section III A, the global custodial $SU(2)$ symmetry is spontaneously broken in (H_{12}). The absence of the custodial symmetry, and the presence of massless Goldstone bosons in the spectrum exclude this phase from phenomenological considerations if one is interested in embedding SM physics in the 2HDM.[4]

Sectors (H_1) and (H_2) are equivalent, and for definitiveness we will work with the latter. This is defined by $\kappa_2 > \kappa_2^c$, $\kappa_1 < \kappa_1^c$, with the field Φ_2 reproducing the SM-like Higgs. At tree-level this model predicts the existence of three degenerate scalar particles, $m_A^2 = m_{H^\pm}^2 = \mu_{11}^2 + \lambda_3 v^2/2$ (see eqs. (4) and (5)). Additionally, since the mass matrix, eq. (6), is diagonal in the inert limit, we identify the SM Higgs with $m_h^2 = \mu_{22}^2 v^2$, and an additional scalar with mass $m_H^2 = m_{H^\pm}^2 + \lambda_4 v^2$.

The study of the phase structure on the lattice, namely the identification of the different sectors from fig. 1, requires a proxy for an order parameter. The different regions are easily identified by monitoring global observables, i.e., volume averaged operators, such as the average plaquette,

$$P = \frac{1}{V} \sum_{x,\mu,\nu} \mathrm{Tr}\, U_{\mu\nu}\,, \tag{14}$$

the squared Higgs-field length,

$$\rho_i^2 = \frac{1}{V} \sum_{x} \det(\Phi_i(x))\,, \tag{15}$$

or the gauge-invariant links

$$L^a_{\Phi_{ij}} = \frac{1}{8V} \sum_{x,\mu} \mathrm{Tr}\Big\{\Phi_i^\dagger(x) U_\mu(x) \Phi_j(x+\hat{\mu}) \theta^a\Big\}, \tag{16}$$

$$L^a_{\alpha_{ij}} = \frac{1}{8V} \sum_{x,\mu} \mathrm{Tr}\Big\{\alpha_i^\dagger(x) U_\mu(x) \alpha_j(x+\hat{\mu}) \theta^a\Big\}, \tag{17}$$

[4] In fact, in order to reproduce the experimentally observed measurements of the SM, the *alignment* limit of the 2HDM (where one of the scalars reproduces the SM Higgs) seems to be favoured [31].

where α_i is the 'angular' part of the quaternion Higgs field, $\Phi_i = \rho_i \alpha_i,\ \rho_i \in \mathbb{R},\ \alpha_i \in SU(2)$. In order to detect the transitions between the sectors in eq. (13) we mostly look at $L_{\alpha_i} \equiv L^4_{\alpha_{ii}}$ since it is a bounded quantity for all values of the couplings [38], and it is the most sensitive to the transitions [54].[5]

Other than finding the regions where the Higgs effect is active, we are also interested in probing the existence of spontaneous symmetry breaking (SSB) of the additional global symmetries in the 2HDM. In order to confirm the occurrence of SSB we modify the partition function by adding an extra term $\varepsilon\mathcal{B}$ to the action,

$$Z_\varepsilon = \int D\phi(x)\, \exp(-S[\phi] + \varepsilon\mathcal{B}), \tag{18}$$

where $\mathcal{B}$ is a term that explicitly breaks the symmetry in question. In the modified theory there is a preferred direction in the group space, such that we get a non-zero value, $\langle\mathcal{O}\rangle_\varepsilon \neq 0$, for any quantity $\mathcal{O}$ that is not invariant under this symmetry. The occurrence of spontaneous symmetry breaking can then be probed by the order parameter $\langle\mathcal{O}\rangle$ defined by the limiting procedure

$$\langle\mathcal{O}\rangle = \lim_{\varepsilon\to 0} \langle\mathcal{O}\rangle_\varepsilon = \begin{cases} 0, & \text{symmetry intact} \\ v, & \text{spontaneous breaking.} \end{cases} \tag{19}$$

In practice, due to the finite volume of the lattice, the definition of the order parameter must be altered to

$$\langle\mathcal{O}\rangle = \lim_{\varepsilon\to 0} \lim_{V\to\infty} \langle\mathcal{O}\rangle_\varepsilon\,, \tag{20}$$

where the thermodynamic limit is taken before the $\varepsilon \to 0$ limit.

In section III A this procedure is considered for studying the spontaneous symmetry breaking of the custodial $SU(2)$ by studying the quantity $L^3_{\alpha_{12}}$ with

$$\mathcal{B} = \mathrm{Tr}\left[\Phi_1^\dagger(x)\Phi_2(x)\theta^3\right]. \tag{21}$$

C. Standard Model physics on the lattice 2HDM

In this work, we examine carefully the spectrum of the BSM scalar states in the 2HDM described in secs. II A and II B, i.e., the model that shares the same custodial symmetry with the SM. We are particularly interested in exploring how the spectrum of these BSM states depends on the cutoff scale. In this procedure, one must embed the SM in this model by tuning the bare parameters to reproduce SM physics. This introduces the notion of a line of partially constant physics (LPCP), on which we fix the values of two dimensionless, renormalized SM quantities, namely, the ratio of the Higgs to the W boson[6],

$$R \equiv \frac{m_h}{m_W}\,, \tag{22}$$

and the renormalized running gauge coupling $g^2_R(\mu)$. The ratio, R, can also be related at tree-level to the renormalized quartic coupling of the corresponding 'broken' scalar, $R^2 \propto \lambda_R/g^2_R$ [55]. In the following, we fix the R-ratio to be close to the SM value, $R = 1.5$, while the renormalized gauge coupling is set to its physical value at the scale of the W boson mass, $g^2_R(\mu = m_W) \equiv 4\pi\alpha_W(\mu = m_W) \sim 0.5$. In other words, we scan the space of bare couplings in eqs. (10) and (11) to study possible values of the BSM scalar masses while keeping R and $g^2_R(\mu = m_W)$ constant. Since no

[5] The quantity ρ_i^2 can be related to the number of scalar states, while the gauge-invariant link can be understood as the energy density of the gauge-Higgs interaction,

$$L^4_{\Phi_{ii}} = \frac{1}{8V}\frac{\partial}{\partial\kappa_i}\log Z.$$

In the Higgs phase, the gauge interaction is screened by the 'condensation' of the scalar field, making the gauge field configurations smoother, and thus increasing the average gauge-invariant link. Heuristically, using the usual symmetry breaking perspective the 'symmetric' phase can be understood as a random state of the $SU(2)$ part of the scalar field, α, while it is in an ordered state in the 'broken' region. This explains why L_α increases across the two regions.

[6] What we call the W bosons in this work are the physical gauge invariant vector states that transform as a triplet under the global $SU(2)$ custodial symmetry group. Their masses can be determined by spectroscopy studies on the lattice. While this is not to be confused with the usual W boson from gauge-fixed perturbation theory (a triplet under gauge symmetry), assuming the validity of the FMS mechanism allows to identify the perturbative states with the physical states.

BSM particles have been found experimentally, it is not of interest to perform tune a complete line of constant physics for the 2HDM by also keeping the masses of the BSM states fixed.

To implement the above strategy involving the LPCP, a scheme for extracting the renormalized gauge coupling has to be specified. For this purpose, we resort to the gradient-flow scheme [56]. In this approach, the renormalized gauge coupling is defined through the action density,

$$\langle E(x,t)\rangle = -\frac{1}{4}\left\langle G^a_{\mu\nu}(x,t)G^a_{\mu\nu}(x,t)\right\rangle \,, \tag{23}$$

where $G_{\mu\nu}(x,t)$ is the flowed gauge field strength tensor,

$$G_{\mu\nu}(x,t) = \partial_\mu B_\nu(x,t) - \partial_\nu B_\mu(x,t) + [B_\nu(x,t), B_\mu(x,t)] \,, \tag{24}$$

with the flowed gauge potential, $B_\mu(x,t)$ satisfying the equation,

$$\frac{\mathrm{d}B_\mu(x,t)}{\mathrm{d}t} = D_\nu G_{\nu\mu}(x,t)\,, \tag{25}$$

with the initial condition $B_\mu(x,0) = A_\mu(x)$. The effect of the gradient flow is to smear the gauge fields over a region of radius $\sqrt{8t}$. In this work, we use the Clover discretization of the field strength tensor, and the Wilson plaquette action for the implementation of the lattice version of eq. (25). For more details, see ref. [57] and references therein.

The action density, eq. (23), at the scale $\mu = 1/\sqrt{8t}$ is a renormalized quantity at finite flow times. It has been computed in perturbation theory [58] in terms of the renormalized coupling g,

$$t^2\left\langle E(t)\right\rangle\Big|_{t=1/(8\mu^2)} = \frac{3(N^2-1)g^2(\mu)}{128\pi^2}\left(1 + c_1 g^2(\mu) + \mathcal{O}\big(g^2\big)\right) \,, \tag{26}$$

with the c_1 being a finite, scheme dependent coefficient, and $N = 2$. Using this relation we define the gradient-flow renormalized gauge coupling, and specify its physical value at the scale of the W boson mass by,

$$g^2_{GF}(\mu) \equiv \frac{128\pi^2}{9}\, t^2\left\langle E(t)\right\rangle\Big|_{t=1/8\mu^2} \,,\;\; g^2_{GF}(\mu = m_W) = 0.5\,, \tag{27}$$

where $\langle E(t)\rangle$ is obtained from the Euclidean spacetime average of $\langle E(x,t)\rangle$. In our lattice calculation, this is obtained by tuning the bare parameters to reproduce the condition,

$$S \equiv \sqrt{8t_0}m_W = 1.0\,, \tag{28}$$

where the t_0/a^2 is the flow time at which $g^2_{GF}(\mu)$ takes the value of 0.5.

Adjusting the bare parameters to satisfy the condition $R = 1.5$ and $S = 1$ at different lattice spacings, a LPCP is mapped out. The interest is then to explore the realizable spectrum of the BSM scalar sector along this LPCP.

D. Physical spectrum & interpolators

In order to study the spectrum of the theory, and also to obtain the first condition for SM physics within the lattice 2HDM, eq. (22), we consider zero momentum, gauge-invariant composite operators at Euclidean time x_4,

$$S^a_{ij}(x_4) = \sum_{\vec{x}} \mathrm{Tr}\left[\Phi^\dagger_i(x)\Phi_j(x)\theta^\alpha\right] \,, \tag{29}$$

$$W^a_{ij,\mu}(x_4) = \sum_{\vec{x}} \mathrm{Tr}\left[\Phi^\dagger_i(x)U_\mu(x)\Phi_j(x+\hat{\mu})\theta^\alpha\right] \,, \tag{30}$$

that can be classified according to the representations of the global symmetry group [59] as well as of the lattice $H(4)$ hypercubic symmetry group. While at any finite lattice spacing it is possible to establish a correspondence between

the $H(4)$ representations and the continuum angular momentum and parity quantum numbers, J^P, in this work we did not try to resolve the different lattice representations, assuming small modifications for the low-lying spectrum. See refs. [60, 61] for a dedicated analysis in the Higgs theory.

At leading order in the lattice spacing S^α_{ij} couples to a $J^P = 0^+$ state for any combination of i, j, and α (with the exception $S^k_{ii} = 0$ due to the properties $\Phi_i^\dagger \Phi_i \propto \mathbb{1}_{2\times 2}$ and $\mathrm{Tr}\,\sigma^k = 0$). On the other hand, the interpolators $W^\alpha_{ij,\mu}$ can be understood in terms of continuum fields by performing a classical expansion in the lattice spacing[7]

$$W^\alpha_{ij,\mu} = \sum_{\vec{x}} \frac{1}{2}\,\mathrm{Tr}\left[\theta^\alpha \left(\Phi_i^\dagger(x)\Phi_j(x) + \Phi_i^\dagger(x)\Phi_j(x) + a(D_\mu\Phi_i)^\dagger\Phi_j - a\Phi_i^\dagger D_\mu\Phi_j\right) + \mathcal{O}\big(a^2\big)\right] . \tag{31}$$

This interpolator sources states with different quantum numbers, depending on the indices i, j, and α. For $i = j$ and $\alpha = 4$ (recall that $\theta^4 = \mathbb{1}_{2\times 2}$), the $\mathcal{O}\big(a^0\big)$ component of $W^4_{ii,\mu}$ couples to a scalar state $J^P = 0^+$, and is the leading contribution. With $i = j$ and $\alpha = 1, 2, 3$, the $\mathcal{O}\big(a^0\big)$ terms on the right-hand side of eq. (31) vanish because $\mathrm{Tr}\,\sigma^k = 0$, and $W^{\alpha=k=1,2,3}_{ii,\mu}$ overlaps with a $J^P = 1^-$ state. In this case, $\mu = 1, 2, 3$ correspond to the $J = 1$ spin components, and $k = 1, 2, 3$ to the $SU(2)$ triplet representation. Finally, when $i \neq j$, the $\mathcal{O}\big(a^0\big)$ component in $W^\alpha_{i\neq j,\mu}$ is always non-zero, and this interpolator primarily couples to four scalar states labelled by α. From the above discussion, we can assign the J^P quantum numbers in the following way,

$$S^4_{ii}\,,\ W^4_{ii} \to 0^+\,, \qquad\qquad W^\alpha_{ij} \to 0^+\ (i \neq j)\,, \qquad\qquad W^k_{ii} \to 1^-\,. \tag{32}$$

Additionally, since the $J = 1$ spin components have the same mass, in the simulations we average over the $\mu = 1, 2, 3$ directions when computing two-point functions.

While the classification of the operators according to the angular momentum representations is straightforward, the connection to the physical spectrum is more involved. The reason is that the spectrum depends not only on the sector of the theory but also on the symmetries of the scalar potential, which can give rise to degenerate or non-degenerate scalar multiplets in the broken phase, and even Goldstone bosons.[8] In this work, we are mostly interested in studying the spectrum in sector (H_2), where both S^4_{22} and W^4_{22} yield the mass of the SM Higgs, m_h, while the vector operator W^k_{22} sources the degenerate $SU(2)-$triplet states that represent the W bosons. The remaining four BSM scalar states are sourced by S^a_{12} or W^a_{12}.

In the (H_2) sector of the custodial 2HDM, the mixing amongst scalar states is absent. This allows us to extract the ground-state energies by computing the effective mass, m_{eff}, from the large Euclidean time behavior of the correlators

$$C_{\mathcal{O}}(x_4) = \langle \mathcal{O}(x_4)\mathcal{O}(0)\rangle = \sum_n \left|\langle n|\hat{\mathcal{O}}|0\rangle\right|^2 e^{-x_4\Delta E_n}\,, \tag{33}$$

where ΔE_n are the energies relative to the vacuum, and $\mathcal{O}$ one of the local interpolators defined in eqs. (29) and (30). The correlation functions are computed with smeared interpolators. For this we consider gradient (Wilson) flow smearing on the gauge links.[9] Additionally, we perform smearing for the scalar fields using the Laplacian operator [62]

$$\begin{aligned}\phi^{(n+1)}(x) &= (1 + r\nabla^2)\phi^{(n)}(x) \\ &= \phi^{(n)}(x) + r\sum_{\mu=1}^{3}\left(\tilde{U}_\mu(x)\phi^{(n)}(x+\hat{\mu}) - 2\phi^{(n)}(x) + \tilde{U}^\dagger_\mu(x-\hat{\mu})\phi^{(n)}(x-\hat{\mu})\right)\,,\end{aligned} \tag{34}$$

where $\tilde{U}$ is the smeared link and r controls the smearing radius. This step is iterated N times, $\phi^{(1)} = \phi \longrightarrow \phi^{(N)}$, corresponding to a smearing radius $\sigma_x \sim \sqrt{2Nr}$.

---

[7] $U_\mu(x) = \exp(iaA^b_\mu\sigma^b/2) = 1 + iaA^b_\mu\sigma^b/2 + \mathcal{O}\big(a^2\big)$ and $\Phi(x \pm \hat{\mu}) = \Phi(x) \pm a\partial_\mu\Phi(x)$.

[8] Notice that in the most general 2HDM there is mixing in the scalar sector, such that a variational method would be required to extract the complete spectrum. This is not the case in the inert limit. On the other hand, mixing always occurs in the sector (H_{12}).

[9] Gradient flow smearing includes smearing in the time direction, which breaks locality in time and may introduce contamination from excited states in the mass extraction. For this reason, the smearing radius was always taken to be very small, $\sqrt{8t_{\mathrm{smear}}} \ll t_{\mathrm{m}}$, where t_{m} is the minimal time in lattice units to measure the effective mass.

III. RESULTS AND DISCUSSION

In this section, we present the results from our numerical study. We start by investigating the spontaneous breaking of the custodial symmetry in phase (H_{12}) in sec. III A. The absence of custodial symmetry in the spectrum in this phase makes it uninteresting for high-energy physics phenomenology. This leaves sectors (H_1) and (H_2) available for constructing BSM models that embed SM physics. We then consider the tuning for the line of constant SM physics, the LPCP described in sec. II C, in the (H_2) sector. The results of this tuning are shown in sec. III B. Section III C gives details of our exploration for the running behaviour of the renormalized gauge coupling along this LPCP. In sec. III D we report our study of the BSM scalar-state spectrum. Finally the finite temperature transition is discussed in sec. III E.

Except for sec. III A, all of the numerical results shown are obtained in sector (H_2). The qualitative structure of the space of parameters, fig. 1, is common for all inert models, as known from our previous works [45, 63]. A detailed study of the phase strucure, the spectrum, and the dependence on the bare couplings, can be found in [44]. For the purpose of this investigation it suffices to monitor the order parameters defined in sec. II B, as well as the mass ratio of the lightest scalar and vector states associated with the SM Higgs and the W bosons, to guarantee that we are working in the desired sector.

A. Spontaneous breaking of custodial symmetry

In this subsection we consider the breaking of the $SU(2)$ global custodial symmetry. In principle, such an investigation can be carried out by identifying massless Goldstone bosons in the sector (H_{12}). This, however, requires a dedicated study of the spectrum in the thermodynamic limit, and is resource-demanding. In this work, we employ a different approach to examine this symmetry breaking pattern by investigating the observable, $L^j_{\alpha_{12}}, j = 1, 2, 3$, defined in eq. (17). This observable is not invariant under the custodial $SU(2)$ transformation. As reported below, through the study of $\langle L^j_{\alpha_{12}} \rangle$ across the boundary between (H_2) and (H_{12}) sectors, we are able to confirm the spontaneous breaking of the custodial symmetry in the latter.

Similarly to what was found[10] in ref. [39], $\langle L^j_{\alpha_{12}} \rangle$ shows large fluctuations with respect to the change of κ_1 when crossing into (H_{12}). An example of $\langle L^3_{12} \rangle$ is demonstrated in the left plot of fig. 2. This means that care has to be taken when using $\langle L^j_{\alpha_{12}} \rangle$ as an order parameter. As a result, conventional methods (susceptibility, Binder's cummulant, etc.) may not be straightforwardly applicable for the investigation of this potential phase transition. In fact, from this plot, it is not possible to draw any reliable conclusion regarding the symmetry breaking pattern. On the other hand, as exhibited on the right-hand side of fig. 2, the plotted quantity, $\langle L_{\alpha_1} \rangle \equiv \langle L^4_{\alpha_{11}} \rangle$, signals non-trivial changes of the system in the passage from (H_2) to (H_{12})[11]. In order to probe the possible occurrence of the SSB of custodial symmetry, we follow the procedure introduced at the end of sec. II B. That is, we perform simulations with an added $SU(2)$-breaking term, $\varepsilon\mathcal{B}$ (eq. (21)) in the action, and extrapolate ε to zero in the thermodynamic limit.

The strategy is to then perform simulations at differentvalues of κ_1 straddling the boundary between sectors (H_2) and (H_{12}) with multiple choices of ε and the lattice volume, L ($L = 32, 44, 64$). The study is carried out at relatively high lattice cutoff, with $\beta = 8.56$ in eq. (11). For other bare couplings that appear in $S_{\rm 2HDM}$ in eq. (10), we set their values to be those in the $\beta = 8.56$ column in tab. I. Results of $\langle L^3_{\alpha_{12}} \rangle$ from these simulations are shown in fig. 3 for $L = 32$ and $L = 64$. Since at any finite ε the system is forced into a unique ground state chosen by the inclusion of the $\mathcal{B}$-term, eq. (21), the expectation value now shows a smooth dependence on κ_1. From the plots in fig. 3, it is evidenced that $\langle L^3_{\alpha_{12}} \rangle$ will extrapolate to a non-zero value in the limit $L \to \infty$ and $\varepsilon \to 0$ when κ_1 is above a certain critical value, κ_1^c, while it may vanish in the regime $\kappa_1 < \kappa_1^c$. It is noted that at large enough κ_1, finite-volume effects are less significant, where it is also seen that the extrapolation in ε is less pronounced at large volume.

The above observations indicate that $\left\langle L^3_{\alpha_{12}} \right\rangle$ in the $L \to \infty$ and $\varepsilon \to 0$ limits can be employed as an order parameter for investigating spontaneous breaking of the global $SU(2)$ symmetry in sector (H_{12}). Following the procedure described

[10] A similar approach was used in this reference to confirm the spontaneous symmetry breaking of the $SU(2) \times SU(2)$-symmetric 2HDM.
[11] This quantity, $\langle L_{\alpha_1} \rangle$, is not an order parameter for the custodial $SU(2)$ since it is invariant under this symmetry transformation.

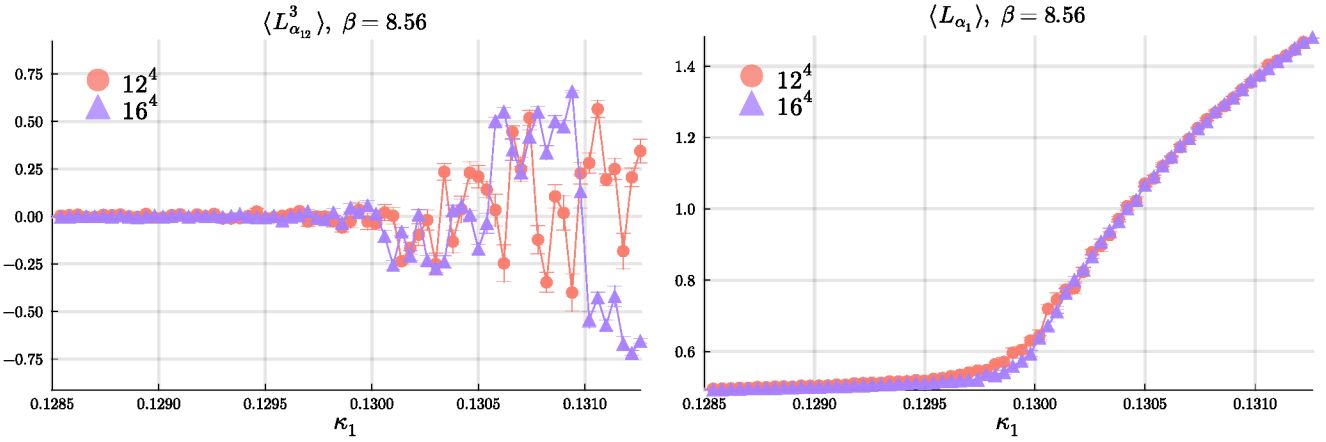

FIG. 2. Expectation values for $L^3_{\alpha_{12}}$ (left) and L_{α_1} (right) as a function of κ_1 signaling the transition between (H_2) and (H_{12}). The constant bare couplings are those from the $\beta = 8.56$ point of the LPCP. Two lattice volumes are shown, 12^4, and 16^4.

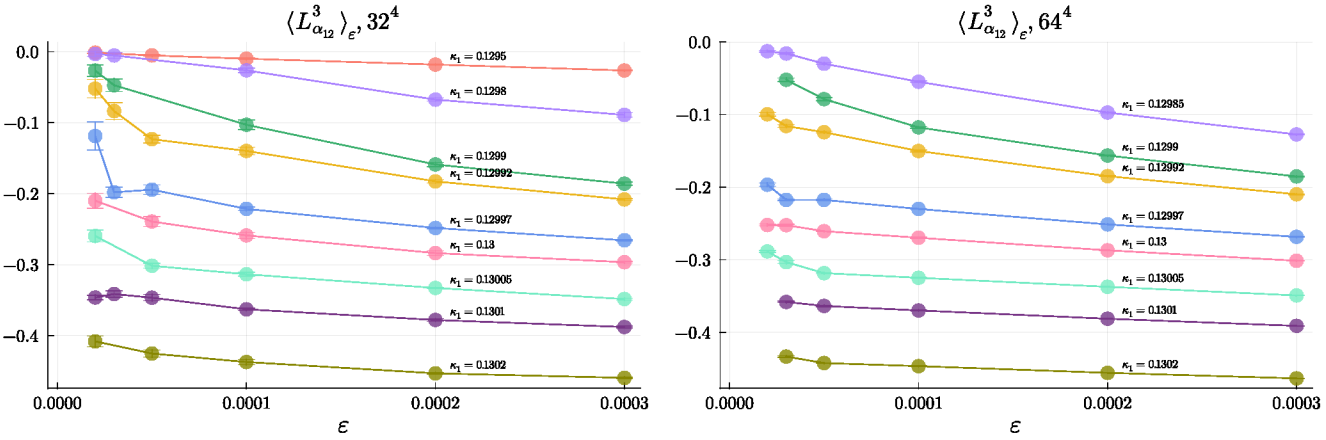

FIG. 3. Expectation value of the $SU(2)$ non-invariant quantity $L^3_{\alpha_{12}}$ as a function of the symmetry breaking parameter ε for different values of the hopping parameter κ_1 below and above the transition. Two different volumes are shown.

in eq. (20), we use our data at $L = 32, 44, 64$ to extrapolate $\langle L^3_{\alpha_{12}} \rangle_\varepsilon$ to the infinite-volume (thermodynamic) limit first at each pair of (κ_1, ε). Results in this limit are demonstrated in fig. 4, where we also show the subsequent extrapolation to $\varepsilon \to 0$ through a linear fit by employing data at the three smallest values of ε for each κ_1[12].

Figure 5 exhibits $\langle L^3_{\alpha_{12}} \rangle$ as a function of κ_1, at $\varepsilon = 0$ and in the thermodynamic limit. Using data points displayed in this plot, we can estimate the value of κ_1^c. In order to do this, we parametrize the κ_1-dependence in the broken phase with a functional form inspired by continuous transitions, that is, $\langle L^3_{\alpha_{12}} \rangle = A(\kappa_1 - \kappa_1^c)^\nu$. The result of the fit to this functional form is also shown in fig. 5, with the parameters $\kappa_1^c = 0.1299053(13)$ and $\nu = 0.5184(80)$. It is important to remark that although we have employed a functional form from continuous phase transitions to parametrize the order parameter in fig. 5, the type of phase transition is not determined.[13] In fact, as will be seen in section III D, the masses of the states in lattice units in the theory generally do not vanish in the infinite volume limit across the $(H_2) \to (H_{12})$ transition, indicating that the correlation length does not diverge, thus excluding the possibility of a second-order phase transition. While the exploratory results in ref. [63] seem to indicate a first-order transition, the assessment of the type of transition is beyond the scope of this work.

[12] The addition of more points in the fit, or the use of a higher order polynomial does not greatly affect the central value of the extrapolation for κ_1 close to κ_1^c. On the other hand, the precise shape of the curve for values farther above κ_1^c is not as relevant for the purpose of this investigation.

[13] The use of this functional form serves only to obtain a rough estimate of κ_1^c, but a precise estimate of this value is not relevant for the study. Similarly, the use of smaller ε would not change the qualitative conclusions but serve only to improve the resolution of the transition.

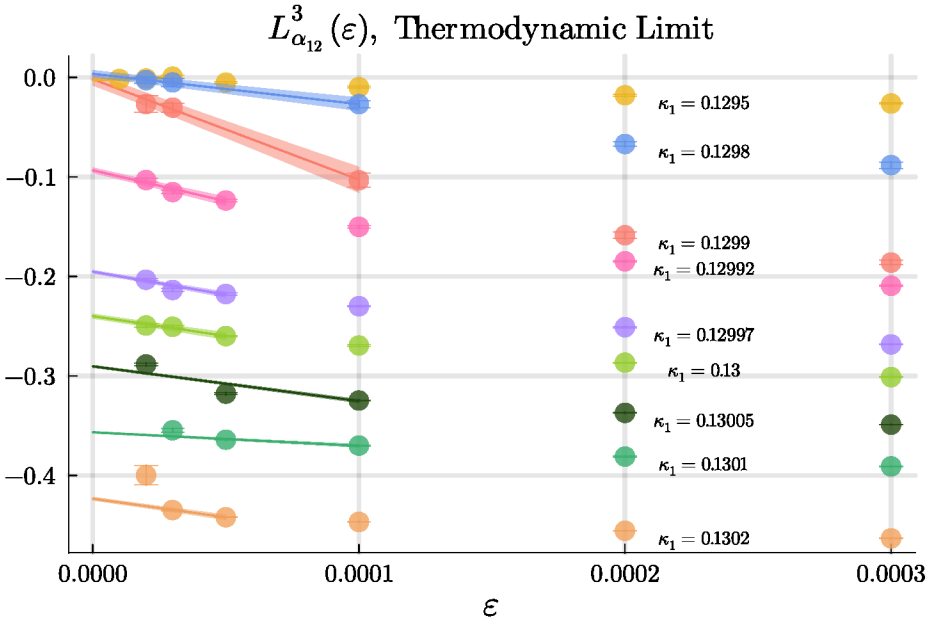

FIG. 4. Expectation value of the $SU(2)$ non-invariant quantity $L^3_{\alpha_{12}}$ as a function of the symmetry breaking parameter ε in the thermodynamic limit for different values of the hopping parameter, κ_1.

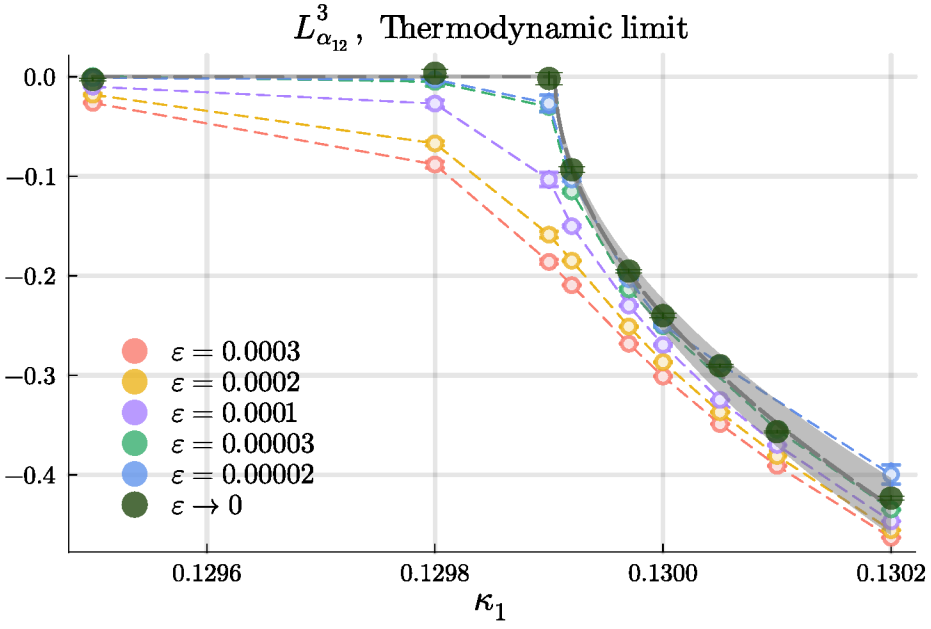

FIG. 5. Order parameter $\langle L^3_{\alpha_{12}} \rangle$ in the thermodynamic limit and with the $\varepsilon \to 0$ extrapolation.

B. Tuning the standard model line of constant physics and setting the scale

In the previous subsection, the absence of the custodial symmetry in the spectrum in sector (H_{12}) was established. It is also known that the Higgs/FMS mechanism is inactive in (H_0). This leaves (H_1) and (H_2) to be the only relevant regimes of the parameter space for model building, since these are the sectors where the SM can be embedded. In this work we consider the LPCP (see sec. II C) in sector (H_2), with $\kappa_2 > \kappa_2^c$ and $\kappa_1 < \kappa_1^c$. This means that the SM

β	8.2	8.3	8.4	8.56	8.64
κ_2	0.13175	0.13104	0.1306	0.1301	0.129985
η_2	0.00338	0.003	0.00285	0.00275	0.002737
R	1.509(94)	1.527(80)	1.494(65)	1.504(39)	1.462(53)
S	1.0055(98)	0.9956(65)	0.994(14)	0.994(20)	0.9958(94)
am_h	0.402(28)	0.363(21)	0.305(16)	0.2192(84)	0.1863(75)
am_W	0.2666(26)	0.2377(15)	0.2041(29)	0.1458(29)	0.1275(11)
t_0/a^2	1.7781(58)	2.1934(74)	2.966(13)	5.810(45)	7.626(43)
$1/a$ (GeV)	301.5(29)	338.2(21)	393.8(57)	551(11)	630.4(56)
$m_W L$	8.485(14)	7.639(13)	6.569(15)	4.694(18)	6.145(17)

TABLE I. Bare couplings β, κ_2, η_2 of the LPCP together with the corresponding physical conditions R, S, the SM masses am_h, am_W in lattice units, the gradient flow scale t_0/a^2 and the estimated cutoff energy $\Lambda_c = 1/a$. The remaining couplings were fixed to the values: $\kappa_1 = 0.1245$; $\eta_1 = 0.003$; $\eta_3 = 0.0002$; $\eta_4 = \eta_5 = 0.0001$. The simulations are performed on lattices with sizes $L = 28, 28, 32, 32, 48$ for the five β values.

states couple to the Φ_2 interpolators as described in sec. II D. Other than the SM states, in this sector we find four non-SM scalar states with masses m_H and $m_A = m_{H^\pm}$. From eq. (32), the correspondence between the interpolators and the states is (the superscript index j runs from 1 to 3)

$$
\begin{aligned}
&S_{22}\,, && \text{SM Higgs } (m_h)\,,\\
&W^j_{22}\,, && W\text{-bosons } (m_W)\,,\\
&S^4_{12}\,,\ W^4_{12}\,, && \text{BSM scalar } (m_H)\,,\\
&S^j_{12}\,,\ W^j_{12}\,, && \text{BSM scalars } (m_A = m_{H^\pm})\,.
\end{aligned}
$$

Our strategy to build the LPCP is to sequentially increase the bare coupling β in eq. (11) towards finer lattice spacing. At each β value, we scan the $\{\kappa_2, \eta_2\}$-space to find parameters such that the SM conditions,

$$R = \left(\frac{m_h}{m_W}\right)_{\text{latt}} = \left(\frac{m_h}{m_W}\right)_{\text{phys}} = 1.5\,, \tag{35}$$

$$S = \left(\frac{m_W}{\mu_0}\right)_{\text{latt}} = \left(\frac{m_W}{\mu_0}\right)_{\text{phys}} = 1.0\,,\ \text{with } g^2_{\text{GF}}(\mu_0) = 0.5\,,\ \text{and } \mu_0 = \frac{1}{\sqrt{8t_0}}\,, \tag{36}$$

are satisfied.[14] Additionally, in this work the lattice spacing in natural units is obtained by

$$a = \frac{(am_W)^{\text{latt}}}{m_W^{\text{phys}}}\,, \tag{37}$$

where $m_W^{\text{phys}} = 80.377(12)$ GeV is the physical value of the W boson mass [7], and $(am_W)^{\text{latt}}$ the corresponding lattice measurement.

While we adjust κ_2 and η_2 to tune for the above SM conditions, the remaining couplings $(\kappa_1, \eta_1, \eta_3, \eta_4 = \eta_5)$ in the action in eq. (10) are fixed to constant values, such that the BSM scalar masses, m_H and $m_A = m_{H^\pm}$, are larger than the SM particle masses, but still well below the lattice cutoff. For this purpose, κ_1 and η_1 are chosen such that the system is well within the (H_2) sector. That is, the value of κ_1 is much smaller than κ_1^c ($\kappa_1 = 0.1245$ and $\eta_1 = 0.003$). Finally, the couplings $\eta_3, \eta_4 = \eta_5$ are kept small ($\eta_3 = 0.0002$, $\eta_4 = \eta_5 = 0.0001$). This guarantees the LPCP to be mostly insensitive to the Φ_1 scalar sector (within the available precision). Notice that while we fix the values of all the BSM bare couplings for the investigation of LPCP in this subsection, later on we will perform scans in κ_1 to explore some limits of the BSM spectrum (see sec. III D below).

For each β value, around ten replicas of $\sim 10K$ HMC trajectories are generated in our simulations. Measurements of the interpolators are performed at each HMC trajectory, while the computation of the gradient flow action density is

[14] It is important to remark that the second physical condition is valid in the $\overline{\text{MS}}$-scheme, and thus our condition is only valid at leading order. However, given the targeted precision and the small values of the couplings, we expect this condition to represent SM physics.

carried out less frequently (the frequency is adjusted for each β value). For the finest lattice the resulting integrated autocorrelation time for the Higgs mass is $\tau_{i,m_h} \approx 3$ molecular dynamics units (MDUs).

The results for renormalization trajectory in the 3-dimensional parameter space spanned by $(\beta, \kappa_2, \eta_2)$ are dispayed in table I . Five β values are considered, with the cutoff, $1/a$ computed from eq. (37), ranging from 300 GeV to 630 GeV. The simulations are performed with large enough volumes, $L = 32, 32, 32, 32, 48$ for the five β values, such that finite volume effects are mitigated. In fact, the value $m_W L$ is always kept above 4 (for this set of couplings, m_W is the lowest mass in the spectrum).

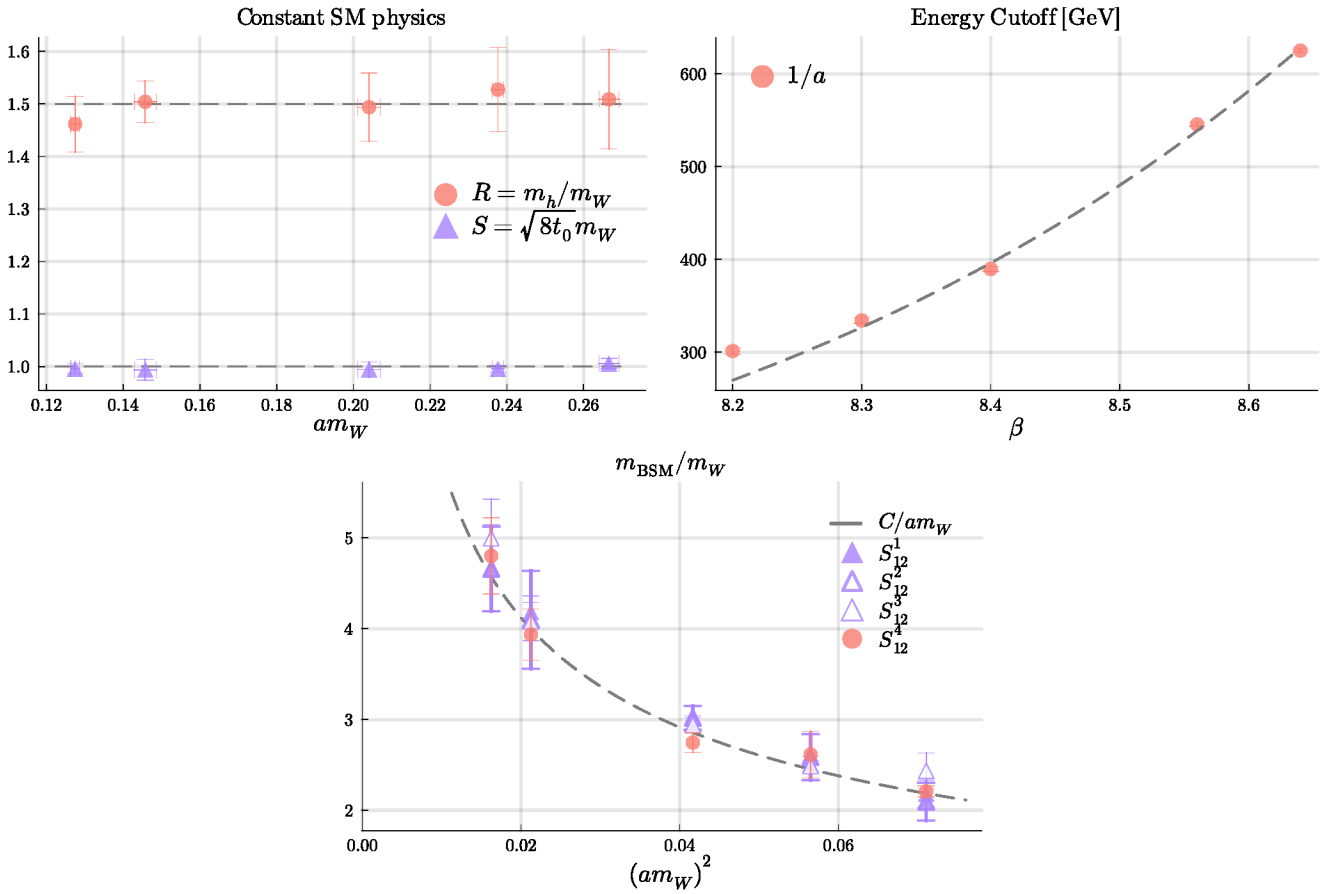

FIG. 6. Data from table I: physical conditions R and S for the selected points in the line of constant SM physics as a function of am_W (left). For decreasing am_W, each points has a corresponding increasing β value. The lattice cutoff, $1/a$, estimated from $a = \hat{m}_W/m_W^{\rm phys}$ is shown on the right as a function of β. The bottom plot shows the ratio of the BSM states $m_{H^\pm} = m_A$ (triangles), and m_H (circle) to the W boson mass for the points in the LPCP. The fit to the functional form C/am_W (dashed line), with C a fitting constant, is only meant to indicate that, within errors, the increase in the ratio $m_{\rm BSM}/m_W$ seems to come mostly from the change in am_W towards the continuum.

Both the physical conditions for R and S in eqs. (35) and (36), and the lattice cutoff, $1/a$, are shown in the upper row of fig. 6 as a function of am_W and β, respectively. The difference in precision of condition R and that of condition S is clear in the left plot. This is because the computation of R involves the measurements of scalar masses. Nonetheless, both conditions are satisfied within errors for all points. On the right-hand side the cutoff seems to follow an exponential dependence in β, as expected in the scaling region.

Since κ_1 is kept fixed in our construction of LPCP, the BSM masses in lattice units are expected to be roughly constant on the five ensembles listed in table I. In fact, it is found that $am_H \approx am_A \sim 0.6$ with large uncertainties. Furthermore, in the bottom plot of fig. 6, the mass ratio between various BSM scalar states and the W boson is shown as a function of am_W. This plot shows that this ratio grows when the lattice spacing becomes finer, since the SM physics is embedded ($R = 1.5$ and $S = 1$) in these five data points. This simply indicates that these points do not define a 'full renormalization trajectory' of the 2HDM. In order to obtain the complete line of constant physics

for this model, it would be necessary to perform further tuning of the remaining BSM couplings, such that at each β value, $m_{\rm BSM}/m_W$ is kept fixed.

The results listed in tab. I show that the quartic coupling η_2 decreases as the cutoff scale increases (or the lattice spacing becomes finer). This seems to be the opposite of what one expects from triviality which predicts that bare quartic couplings grow when the lattice spacing becomes finer along a line of constant physics, and eventually diverge before the continuum limit is reached [64]. This could, at the first glance, suggest the existence of a non-perturbative, non-trivial fixed point with renormalized $\eta_2 \neq 0$ in the continuum. However, it is important to remark that triviality is usually framed within mass-independent renormalization schemes for examining the properties of the quartic couplings. Contrarily, in this work we set up a LPCP non-perturbatively, using a renormalization scheme that is inherently massive. Such a scheme may lead to a different running behaviour of the quartic coupling compared to that in a mass-independent scheme. A clear example will be seen in the following subsection where we study the running of the gauge coupling. We leave a dedicated, non-perturbative investigation of triviality in gauge-Higgs theories for our future work.

C. Running gauge coupling

In this work, the running of the renormalized gauge coupling is studied in the gradient-flow scheme defined through the action density, as described in eq. (27). Results of $g^2_{GF}(\mu = 1/\sqrt{8t}; \beta)$ for all five β values listed in table I are exhibited in fig. 7 as a function of the energy scale, μ, relative to m_W. For each lattice spacing, we only show results at $\mu a < 0.5$, corresponding to $t/a^2 > 0.5$, since lattice artefacts can be large for those at smaller flow time. Figure 7 demonstrates that $g^2_{GF}(\mu = 1/\sqrt{8t}; \beta)$ obtained at different β values are compatible in a large range of μ/m_W, with significant lattice artifacts being observed only near $t/a^2 = 0.5$. Notice that in the tuning for the LPCP, the uncertainty in the 'mass condition', R, is larger than that in S, as shown in fig. 6. However, the results in fig. 7 seem to indicate that effects of the potential mistuning of the masses are negligible in this quantity.

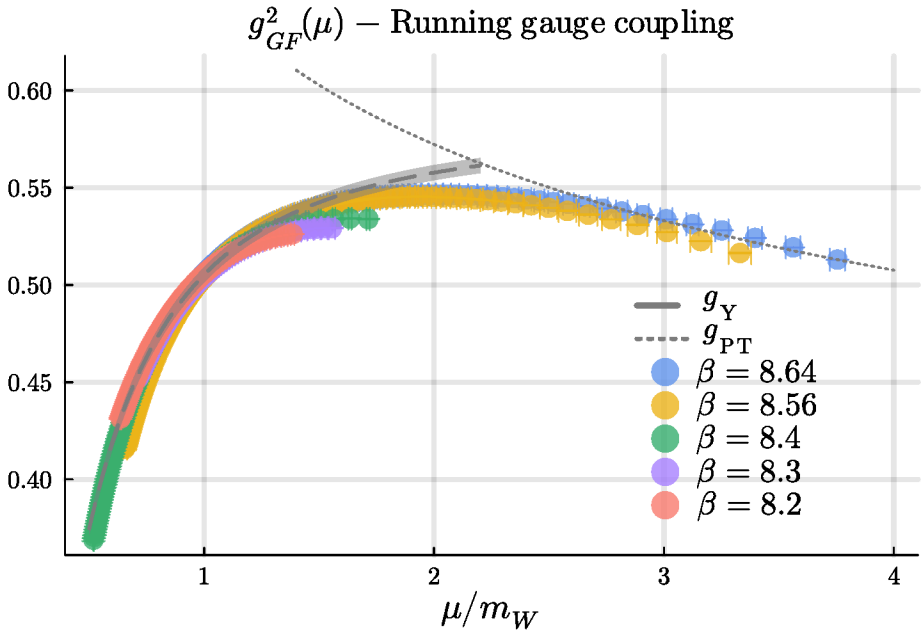

FIG. 7. Running behaviour of the gauge coupling, $g^2_{GF}(\mu)$, from lattice simulations along the LPCP in table I. Only results with $\mu a < 0.5$ are shown. The one-loop perturbative prediction, $g^2_{\rm PT}$, is matched to $g^2_{GF}(\mu)$ computed at $\beta = 8.64$ at $\mu/m_W \approx 3.5$. The gauge coupling from the Yukawa potential is fitted in the infrared region, with the estimated screening mass $m_{\rm screen} = 0.6243(28)m_W$.

We can compare our numerical study with the prediction of perturbation theory, where the latter is expected to be valid, that is, at large μ. In fig. 7 the one-loop perturbative result, $g^2_{\rm PT}(\mu)$, is also shown. The value of $g^2_{\rm PT}(\mu)$ is

first matched to that of $g^2_{GF}(\mu)$ computed on the $\beta = 8.64$ ensemble in table I, at a renormalization scale well above m_W. We choose this matching scale to be $\mu \approx 3.5 m_W$. The running behaviour of $g^2_{\rm PT}(\mu)$ is then obtained from the one-loop β-function,

$$\beta_{SU(N)+\text{Scalars}} = \mu \frac{\mathrm{d}g}{\mathrm{d}\mu} = -\frac{b_0 g^3}{16\pi^2} + \mathcal{O}(g^5)\,, \quad b_0 = \frac{22N - n_s}{6}\,, \tag{38}$$

where $n_s = 2$ is the number of scalar-field doublets, and $N = 2$ for $SU(2)$ gauge theory. Notice that the lattice data and the perturbative curve overlap only in a limited range since the massless perturbative scheme is only valid at very large μ. To further extend this overlapping regime, one has to perform lattice simulations at finer lattices, which is beyond the scope of this work.

The behaviour of the running gauge coupling presented in fig. 7 can be understood as follows. When the renormalization scale is well above m_W, the gauge bosons are effectively massless. Consequently, the gauge coupling decreases as we increase the scale. The theory is then QCD-like, with the onset of asymptotic freedom at large μ. When the energy scale approaches m_W from above, the masses of the gauge bosons become relevant and the coupling stops increasing. The screening effect on the gauge force due to the massive W boson is evident at intermediate values of μ, where we observe significant difference between $g^2_{\rm PT}$, obtained in a mass-independent scheme, and $g^2_{GF}(\mu)$, computed in a mass-dependent scheme. Notice that this effect is already relevant around $\mu/m_W \approx 2$, where $g^2_{GF}(\mu)$ exhibits very mild dependence on μ.

In the low-energy regime where $\mu \ll m_W$, the gauge boson is expected to decouple completely. Here the model effectively becomes a scalar field theory, and the coupling decreases with μ, as can be seen in fig. 7. In this region, the gauge interaction can be characterized by an Yukawa-like potential [55, 65]. In fact, the first lattice studies of the gauge coupling in $SU(2)$-Higgs models were carried out using the static potential of a pair of external $SU(2)$ charged doublets. For large enough separations of the charges, the potential is expected to be Yukawa-like due to the exchange of a massive boson. In the continuum the potential is given by the integral

$$V_{\rm Y}(r) = \int \frac{d^3k}{(2\pi)^2} \frac{e^{ik\cdot r}}{k^2 + m^2} = \frac{1}{4\pi r} e^{-mr}\,, \tag{39}$$

involving the propagator of the massive boson. We use this to describe the running gauge coupling at $\mu \ll m_W$,

$$g^2_{\rm Y}(\mu) = r^2 \frac{\mathrm{d}V_{\rm Y}}{\mathrm{d}r}\bigg|_{\mu=1/r}\,, \tag{40}$$

whose functional form can be employed to fit the lattice data. The result of the fit for the finest lattice is shown for the low-energy region in fig. 7, with the corresponding Debye *screening-mass* estimated to be $m_{\rm screen} = 0.6243(28) m_W \approx 50$ GeV. The relevant point here is the qualitative agreement between the running behaviours of $g^2_{\rm Y}(\mu)$ and $g^2_{GF}(\mu)$ for scales up to m_W. On the other hand, although it may be related to the W mass, [55, 66], the screening-mass obtained from the fit is not a physical quantity.[15]

D. Spectrum of scalar states beyond the standard model

The tuning for the LPCP in tab. I is performed by adjusting the set of three bare couplings, $\{\beta, \kappa_2, \eta_2\}$, spanning the parameter space for the SM Higgs sector in the presence of $SU(2)$ gauge fields. In this procedure, all the other couplings (the BSM couplings) were held fixed, as explained in sec. III B. The values of these BSM couplings actually have profound implications for the phenomenology of the custodial 2HDM under investigation. This subsection describes our exploration of physically realizable scenarios by varying them, while keeping to the LPCP. In particular, we are interested in the objective of establishing non-perturbative bounds on the BSM spectrum of this model. This would, in principle, require a scan in the space of all the remaining parameters, $\{\kappa_1, \eta_1, \eta_3, \eta_4\}$, while maintaining the conditions of eqs. (35) and (36). The computational cost of this scan and the requirement of retuning for the

[15] This screening mass clearly depends on the choice of renormalization scheme.

LPCP make it a challenging task. Consequently, for our first step of investigating the custodial 2HDM reported in this article, the BSM quartic couplings, $\eta_{1,3,4}$, are fixed to be weak, with the values used in our tuning for the LPCP (sec. III B). We then explore the effect of changing the hopping parameter of the 'unbroken' scalar, κ_1, within the sector (H_2). In principle, varying κ_1 should require the retuning of $\{\beta, \kappa_2, \eta_2\}$. However, since $\eta_{1,3,4}$ are kept small, SM physics is expected to be almost insensitive to the change of κ_1.

Before presenting details of our numerical results on the masses of the BSM scalar states, we notice that some qualitative features of the spectrum can be obtained using perturbative results in eqs. (4) to (6), since our calculations are performed in the regime of weak quartic couplings. We expect that the states A and $H^{\pm}$ are degenerate. The difference between their mass and that of H is dominated by the size of η_4. All these masses should decrease with increasing κ_1 in sector (H_2). Furthermore, when $\kappa_1 > \kappa_1^c$, the model is in sector (H_{12}) and the $SU(2)$ custodial symmetry is spontaneously broken (sec. III A), where the three degenerate states become Goldstone modes. The above considerations indicate that we can search for a qualitative lower bound of the BSM masses in sector (H_2) with κ_1 close to κ_1^c. A more detailed, precise search for this lower bound should be carried out by also varying η_4, which we leave for future work.

β	8.2	8.3	8.4	8.56	8.64
κ_1^c	0.13089(31)	0.13018(42)	0.13021(65)	0.12996(59)	0.12965(61)

TABLE II. Transition points, κ_1^c, between sector (H_2) and (H_{12}) for the points in table I, obtained from hysteresis cycles in L_{α_1}. The errors are estimated from the width of the hysteresis curve

In order to perform scans in the (H_2) sector only, we first determine κ_1^c for each β value in tab. I, through examining thermal cycles. This is carried out by changing slightly κ_1 after performing a small number of HMC updates, and then continuing the simulations. Implementing a sequence of such changes, one can increase and then decrease κ_1 across the boundary between sectors (H_2) and (H_{12}). This thermal cycle leads to hysteresis effects on the global observables such as L_{α_1}, from which the location of the phase transition can be estimated. The results for κ_1^c are summarized in table II. Notice that for $\beta = 8.56$ this rough estimate agrees with the computation from section III A.

Knowing κ_1^c for each β, we then perform simulations at different choices of κ_1 around κ_1^c, holding the values of all the other couplings and lattice volumes fixed to those in tab. I. To ensure that we stay on the LPCP when the simulations are carried out in the (H_2) sector, the SM conditions, eqs. (35) and (36), are monitored. Figure 8 shows the results of these conditions from the scan of κ_1. From this plot, we see that the values of R and S remain compatible with those for the LPCP tuned in sec. III B. In other words, taking into account the uncertainty of κ_1^c exhibited in table II, one concludes that the SM conditions are still satisfied within error in sector (H_2) for the values of κ_1 we investigated. This can be qualitatively understood as a property of the model in the regime of weak quartic couplings, and the current study is indeed performed in this regime. Nevertheless, we note that the LPCP in table I is defined with κ_1 far away from κ_1^c, while the points shown in fig. 8 are around the transition point. It is then interesting to see that the SM conditions remain valid with such a large variation of κ_1. Finally, for $\kappa > \kappa_1^c$ the theory is in sector (H_{12}), and the SM conditions are not expected to be valid.

In addition to R and S, we also examine the masses of the Higgs and W bosons in the above scan of κ_1. We exhibit these results in the left plot of fig. 9, where the κ_1 values are those appearing in fig. 8. As can be seen in this plot, these masses in lattice units are compatible with those on the LPCP in tab. I. We notice that at the largest κ_1 for each bare gauge coupling, am_h and am_W increase slightly, while their ratio, R, remains consistent with that at other κ_1 values in the scan. To investigate this phenomenon further, we study the κ_1 dependence of the cutoff scale. The right plot of fig. 9 shows the cutoff scale, $1/a$, estimated from the condition $S = \sqrt{8t_0}m_W = 1$ with m_W set to its physical value. This plot demonstrates that the cutoff decreases when κ_1 reaches large enough values, and indicates that the increase in am_h and am_W derive from the change in the lattice spacing. Notice, however, that due to the uncertainty in κ_1^c, these points with a decreasing cutoff scale may already be in sector (H_{12}), where one cannot embed the SM in the model. [16]

The key conclusion is that the SM conditions, and thus the LPCP, remain unchanged within sector (H_2) when κ_1 is varied. As will be described in detail below, the masses of the BSM scalar states, $m_{H,A,H^{\pm}}$, decrease by roughly one

[16] The improved estimate of κ_1^c for $\beta = 8.56$ in section III A further confirms this.

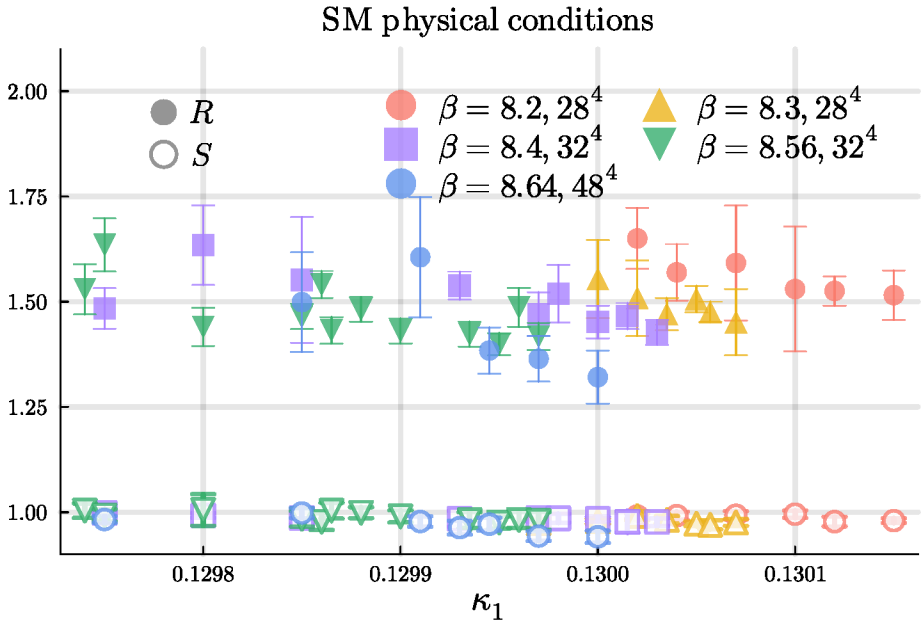

FIG. 8. Standard Model conditions eqs. (35) and (36) for simulations at different κ_1 with other couplings fixed to the values in table I.

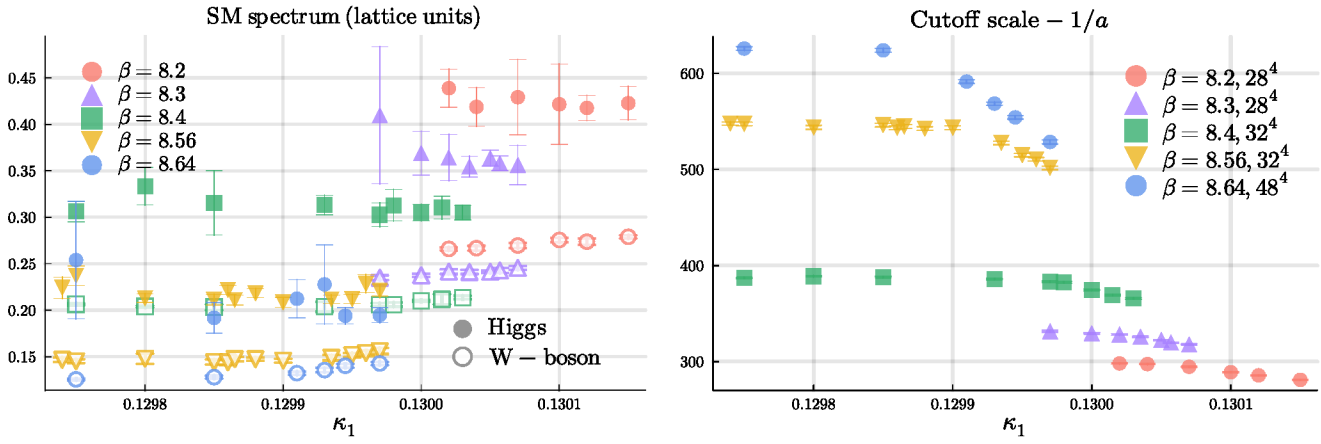

FIG. 9. Left: Higgs and W boson masses in lattice units as a function of κ_1 corresponding to the simulations in fig. 8. Right: Cutoff energy estimated from the condition $S = \sqrt{8t_0}m_W = 1$, with m_W set to the experimental value.

order of magnitude to become smaller than m_W when κ_1 is varied from 0.1245 (its value in tab. I) to $\sim \kappa_1^c$. This leads to the expectation that the BSM dynamics of the model in the region near κ_1^c can be quite different from that in the regime wherethe LPCP tuning is carried out, but it is interesting to see that due to the weakness of the quartic coupling, the SM conditions are still valid at $\kappa_1 \lesssim \kappa_1^c$.

Next, we investigate the spectrum of the BSM scalar states for all κ_1-scanning points in fig. 8. Figure 10 shows the ratios between the masses of these states and m_W for all values of β in tab. I. Here we stress again that the values of κ_1 in this figure are close to κ_1^c, and are much larger than that ($\kappa_1 = 0.1245$) used to tune the LPCP in table I. Comparing the results exhibited in figs. 6 and 10, we see significant changes in the BSM scalar masses when varying κ_1. It is also obvious that the mass difference between the H and A, $H^\pm$ is clearly observed when κ_1 is close to κ_1^c, while these four states appear to be degenerate within error in fig. 6. Since all the bare quartic couplings are small in this work, one can understand this qualitatively from the tree-level perturbative result in eq. (6), which demonstrates that this mass difference can be attributed to the additive effect of a non-vanishing η_4. Being an additive effect, it is

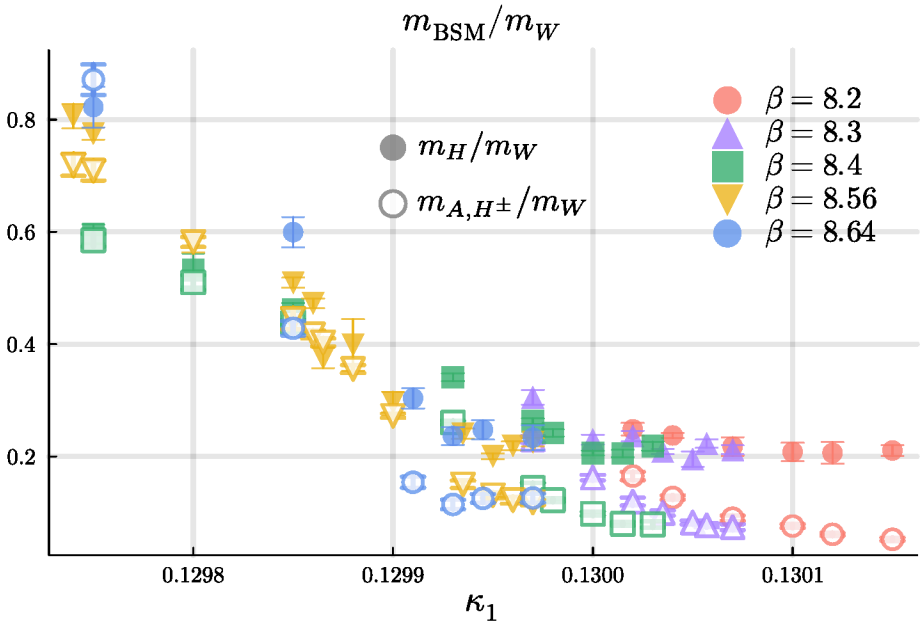

FIG. 10. Mass ratio between the BSM states, $m_{S^4_{12}} = m_H$, $m_{S^j_{12}} = m_A = m_{H^\pm}$, and the W boson, m_W, for the points in fig. 8 at different κ_1 below κ_1^c.

then expected to be more pronounced when the BSM scalar masses are smaller. It should also be mentioned that the data in fig. 10 are obtained at a higher precision compared to those in fig. 6.

One salient feature in fig. 10 is that m_H/m_W develops a plateau when κ_1 approaches κ_1^c in sector (H_2). This offers evidence for a non-zero lower bound for m_H in this sector. We estimate this lower bound for each β value by fitting the data points near κ_1^c in fig. 10 to a constant. Results of these fits are displayed in tab. III. Contrary to the behaviour of m_H/m_W, it can be seen that $m_{A,H^\pm}$ continues to decrease with increasing κ_1. This is expected since these states become the Goldstone bosons in sector (H_{12}), in the regime $\kappa_1 > \kappa_1^c$. It is also observed that while the plateau value of m_H seems cutoff-independent, the masses of the other three states increase with the cutoff near the transition.

β	8.2	8.3	8.4	8.56	8.64
m_H/m_W	0.209(12)	0.2115(43)	0.2080(37)	0.2111(39)	0.2271(83)

TABLE III. Estimated lower bound for the mass ratio of the BSM H state to the W boson, m_H/m_W, with the values of the quartic couplings and κ_2 fixed to those in tab. I.

In the regime where κ_1 is near κ_1^c in sector (H_2), the BSM scalar states can be much lighter than the SM particles. Therefore, it is important to check that finite-volume effects are under control. We illustrate this using the case of $\beta = 8.64$. For this lattice bare gauge coupling, the LPCP discussed in sec. III B is tuned using the lattice size $L = 48$, as shown in tab. I, where we also report $m_W L \sim 6$. This lattice size should be enough to keep finite-size effects in check for the case in tab. I, where the W boson is the lightest state in the spectrum, as indicated by fig. 6. However, for κ_1 approaching κ_1^c in fig. 10, the BSM scalar states are lighter than the W boson, while the lattice size is also chosen to be the same as that in tab. I. For the case of $\beta = 8.64$ and $\kappa_1 = 0.12991$, the mass of the lightest BSM state is about 15% of m_W, resulting in a small $m_{\rm BSM} L \sim 1 < m_W L$. Using the results at this κ_1 value to investigate the finite-size effects, simulations at four other lattice volumes, $L = 32, 40, 64, 72$, are performed. Figure 11 shows the volume dependence of $m_{\rm BSM}/m_W$ at $\beta = 8.64$ and $\kappa_1 = 0.12991$. It can be observed that m_H/m_W exhibits mild dependence on L, indicating that, at least within errors, volume effects are under control for this mass ratio. On the other hand, the situation is different for the states A and $H^\pm$, where their masses show clear volume dependence.[17] In

[17] Notice that three masses should be degenerate within statistical error, but only in the infinite-volume limit. Finite-size effects can break this degeneracy.

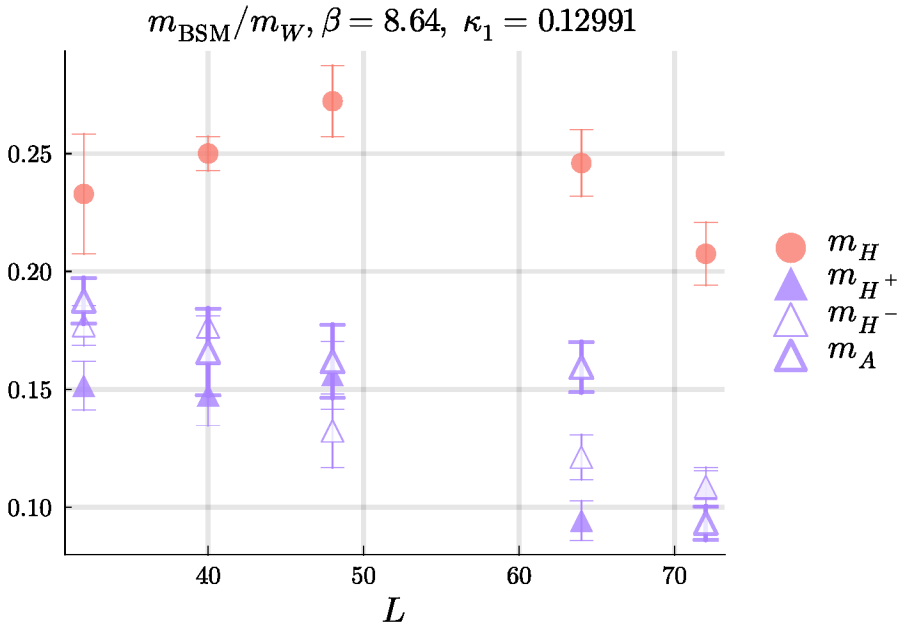

FIG. 11. Lattice-size dependence of $m_{\rm BSM}/m_W$ at the $\beta = 8.64$ and $\kappa_1 = 0.12991$, with all other couplings fixed to their LPCP values in tab. I). The three degenerate scalars (triangles) are displayed separately.

sector (H_2) these states are massive, and the expected volume dependence is exponential $\mathcal{O}(e^{-mL})$. Indeed, infinite-volume extrapolations are investigated using a massive-like exponential function or a massless-like power law [67]. Both procedures lead to non-vanishing but small $m_A = m_{H^\pm}$ in the infinite-volume limit in sector (H_2) when κ_1 is close to κ_1^2. This is exactly what is expected, since only in (H_{12}) these three states become Goldstone bosons.

E. Finite temperature transition

In this subsection we investigate the custodial 2HDM at finite temperature on the LPCP tuned in section III B. In order to study the temperature dependence we perform simulations using the bare couplings in table I and asymmetric lattices with sizes $L^3 \times L_4$, where the temporal extent, L_4, defines the physical temperature $T = 1/(aL_4)$. The lattice sizes at the corresponding β values are summarized in tab. IV.

β	L	L_4
8.2	28	2,3,4,5,6,7,8
8.3	28	2,3,4,5,6,7,8
8.4	32	2,3,4,5,6,7,8,10
8.56	32	2,3,4,5,6,7,8,10,12,14,16
8.64	48	2,3,4,5,6,7,8,10,12,16,20

TABLE IV. Finite temperature simulations for each β value in the LPCP. The spatial extent L and temporal extent L_4 are shown for each β. The values of the remaining couplings are listed in table I.

Since we are interested in studying the 'symmetry restoration' that deactivates the Higgs/FMS mechanism, we examine the observables ρ_2^2 and L_{α_2} defined in eqs. (15) and (17), which signal the transition from (H_2) to (H_0). For each value of β in the LPCP (table I), simulations at different time extents can be employed to probe temperature-dependent properties of these two observables, generically denoted as $\mathcal{O}(T)$ in this subsection. Contrary to the masses obtained from the lattice correlation functions, quantities such as ρ_2^2 or L_{α_2} need to be renormalized. Since the exact renormalization of $\mathcal{O}$ is beyond the scope of this work, we examine the ratio, $\langle\mathcal{O}(T)\rangle/\langle\mathcal{O}(0)\rangle$, in which the multiplicative renormalization of the operator cancels. This quantity can then be compared for different β, with

possible differences being due to lattice artifacts and effects arising from the mistuning and the mismatch of the BSM spectrum in the LPCP.

Figure 12 exhibits the ratios $\langle L_{\alpha_2}(T)\rangle/\langle L_{\alpha_2}(0)\rangle$ and $\langle \rho_2^2(T)\rangle/\langle \rho_2^2(0)\rangle$ as functions of the dimensionless quantity m_W/T, with am_W taken from its zero-temperature values in tab. I. Notice that since the temperature increases with the approach to the continuum at fixed L_4, larger values of β provide access to larger temperatures. In the left plot, results for $\langle L_{\alpha_2}(T)\rangle/\langle L_{\alpha_2}(0)\rangle$ at various β values show small or moderate differences in the regime $T < m_W$. At high-temperature, this difference becomes more sizable since the simulations are carried out at small L_4, resulting in large lattice artefacts whose effects are particularly significant at $L_4 = 2$. On the other hand, $\langle \rho_2^2(T)\rangle/\langle \rho_2^2(0)\rangle$, as displayed in the right plot, shows much more significant discrepancies at different lattice spacings. This can be understood by the fact that ρ_2^2 still needs to be additively renormalized, while L_{α_2} does not. For this reason, below we will only use $L_{\alpha_2}(T)$ to study the phase transition.

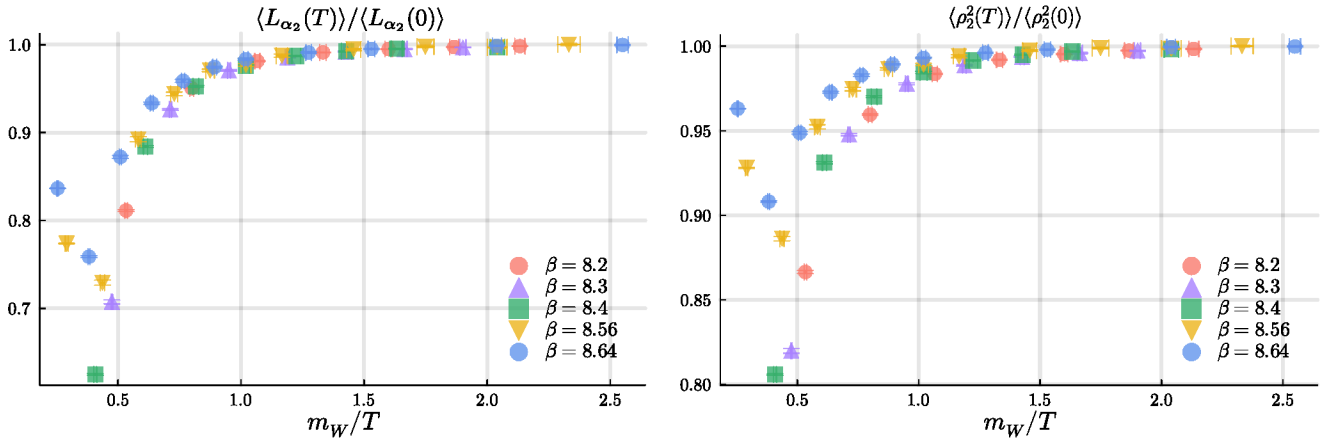

FIG. 12. Finite-temperature dependence of $\langle L_{\alpha_2}(T)\rangle/\langle L_{\alpha_2}(0)\rangle$ (left) and $\langle \rho_2^2(T)\rangle/\langle \rho_2^2(0)\rangle$ (right) on the LPCP at different β values in tab. I.

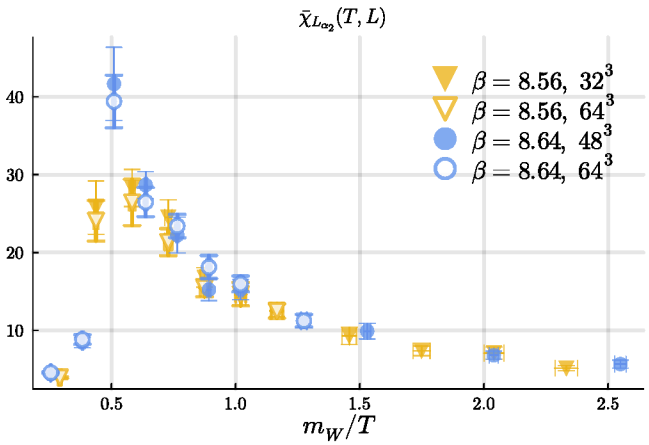

FIG. 13. Finite-temperature dependence of the ratio of the normalized susceptibility, $\bar{\chi}_{L_{\alpha_2}}$, defined in eq. (42). Data at two different spatial volumes are shown for each of the two largest β values.

From fig. 12, one can conclude that a finite-temperature transition occurs around $m_W/T_c \sim 0.5$, where T_c is the critical temperature. In order to better resolve the transition point, and to understand the character of this phase transition we resort to the susceptibility of L_{α_2},

$$\chi_{L_{\alpha_2}}(T, L) = L^4 \left(\langle L_{\alpha_2}^2(T, L)\rangle - \langle L_{\alpha_2}(T, L)\rangle^2 \right) , \tag{41}$$

at various temperatures and lattice volumes. In the above definition, we make the volume dependence in $L_{\alpha_2}(T)$ explicit by denoting it as $L_{\alpha_2}(T, L)$. Again, to avoid dealing with the issue of renormalizing the operator L_{α_2}, we

compute the "normalized susceptibility" defined as

$$\bar{\chi}_{L_{\alpha_2}}(T,L) \equiv \frac{\chi_{L_{\alpha_2}}(T,L)}{\chi_{L_{\alpha_2}}(0,L)} = \frac{\langle L^2_{\alpha_2}(T,L)\rangle - \langle L_{\alpha_2}(T,L)\rangle^2}{\langle L^2_{\alpha_2}(0,L)\rangle - \langle L_{\alpha_2}(0,L)\rangle^2}\,. \tag{42}$$

Figure 13 demonstrates the temperature dependence of $\bar{\chi}_{L_{\alpha_2}}(T,L)$. In this plot, we only show results from the two largest β values in tab. IV. This is because for coarser lattices, either the data points in the regime of $m_W/T \sim 0.5$ are expected to suffer from significant effects of lattice artefacts ($\beta = 8.4$), or there are no data points in this transition regime ($\beta = 8.2$ and 8.3). For each of the β value shown in this figure, we perform an additional simulation at a larger spatial volume.

Results in fig. 13 indicate that the critical temperature (the location of the peak for $\bar{\chi}_{L_{\alpha_2}}(T,L)$ as a function of m_W/T) exhibits mild lattice-spacing dependence. The same behavior was also found previously on a lattice study for the single-Higgs-doublet model [6]. In any case, our data demonstrate that the critical temperature is approximately

$$T_c \sim \frac{m_W}{0.5} \approx 160 \text{ GeV}\,. \tag{43}$$

We stress that the purpose of this work is not to determine T_c, and the result in the above equation should be regarded as a rough estimate. Instead, the relevant information from fig. 13 is the absence of significant volume dependence in the susceptibility. This strongly implies that the transition is a crossover. Our finding for the finite-temperature transition in this custodial 2HDM at weak quartic couplings is then compatible with that in the SM, where previous lattice investigations [6, 68] concluded for a crossover at $T_c = 159.5(15)$ GeV.

Perturbatively, most studies [29–31, 69] suggest that large quartic couplings (equivalently, a large mass splitting in the BSM scalar sector) are needed for the finite-temperature phase transition to be first-order in 2HDM. In this sense, although the lattice cutoffs considered in this work are not large enough to accurately resolve the electroweak transition in the inert 2HDM, our results provide a non-perturbative confirmation that indeed, small quartic couplings do not lead to a first-order transition. There are, however, recent perturbative predictions [31] for a first-order thermal phase transition in the 2HDM for degenerate BSM scalars with masses around 350 GeV. It turns out that these conditions for the mass spectrum are satisfied for the two finest lattices in this study (the BSM scalar masses are shown in fig. 6). Nevertheless, we observe no sign of first-order transition in our non-perturbative lattice investigation.

IV. CONCLUSION AND OUTLOOK

This paper presents the first step of our research programme on non-perturbative investigations of the custodial 2HDM using the techniques of lattice field theory. While our eventual goal is to work in the scenario of strong *renormalized* quartic couplings, as a first step, however, we start with the regime where all the quartic couplings are weak. This strategy enables the initial calibration of the theory by understanding its non-thermal phase structure, and facilitates the study of the theory without dealing with any triviality issues. It also allows us to set the stage for the exploration of the following three crucial issues. First, for the custodial 2HDM to be realized in nature, it has to be able to reproduce the low energy SM observations. Second, it is of interests to the community of particle physicists to gain knowledge on the bounds of the masses of the BSM scalar states. Last, it is essential to understand whether there is a strong first-order EWPT in 2HDM. Althought there have been many perturbative studies of the above issues, a non-perturbative, first-principle investigation is still desirable.

In the work reported here, we consider the parameter space of the custodial 2HDM that can be divided in four sectors, as summarized in fig. 1. Similarly to the case of the SM, most of these regions can be connected through crossover transitions, and therefore do not define truly different phases of the model. Among the four, (H_0) corresponds to the confining region, while the Higgs/FMS mechanism is active in (H_1), (H_2) and (H_{12}). Contrary to the SM, the additional degrees of freedom in this model allow for spontaneous symmetry breaking to occur. In order to probe this and understand in detail the properties of the global symmetries, we examine the order parameter, $\langle L^3_{\alpha_{12}}\rangle$, defined in eq. (17). This order parameter can be employed to probe the $SU(2)$ custodial symmetry, which is shown to be spontaneously broken in (H_{12}) through our careful study described in sec. III A. This means that if we want to keep the $SU(2)$ custodial symmetry, only sectors (H_1) and (H_2) are viable for model building purposes. That is, it is possible to embed the SM in the custodial 2HDM only in these two sectors. Since (H_1) and (H_2) are exactly the same modulo naming conventions, we choose to work in (H_2) in this project.

To study the embedding of the SM in the (H_2) sector of the custodial 2HDM, we consider a 'line of partial constant physics', acronymized as LPCP throughout this article, that is defined to be a line in the bare parameter space, on which the SM physics is realized at different (high enough) cutoff scales. To be more precise, two conditions involving only SM particles and interactions are being kept. The first is the ratio between the Higgs and W boson masses, and the second is the value of the renormalized gauge coupling. These conditions are given in eqs. (35) and (36). The first non-trivial task in our non-perturbative investigation of the 2HDM is to confirm that such a LPCP does exist. Working with the scenario of weak quartic couplings makes the task simpler, and it is why we choose to perform our first study in this regime. In sec. III B, we show that this can be achieved by adjusting the bare gauge coupling, as well as the other two couplings that involve only the SM Higgs doublet, namely, κ_2 and η_2 in the action in eq. (10). All the other bare couplings (the BSM couplings) are kept fixed in this tuning procedure. It is demonstrated that we can obtain a LPCP for five different cutoff scales straddling between 300 and 630 GeV. Details of this LPCP are listed in tab. I.

For the tuning of LPCP, we employ the gradient-flow scheme to define the renormalized gauge coupling, g^2_{GF}. Interesting features are expected for the running behaviour of the coupling in this mass-dependent scheme, since we work in the Higgs phase (H_2) where the gauge bosons are massive. Section III C illustrates our exploration of this issue. As shown in fig. 7, at renormalization scales that are much larger than m_W, g^2_{GF} behaves in a similar way as the QCD coupling, exhibiting asymptotic freedom. Its running can be well described by the mass-independent one-loop $\beta-$function given in eq. (38). At energy scales around $2.5m_W$, where effects from the screening of the gauge force due to the W boson mass are relevant, g^2_{GF} starts to deviate from the one-loop mass-independent running behaviour. In the regime where the renormalization scale is below m_W, the characteristics of its energy dependence can be captured by a Yukawa-like potential. We stress that our work is the first time the gradient-flow gauge coupling is studied in a Higgs phase of gauge-scalar theories.

The aforementioned LPCP is obtained at fixed bare BSM couplings, which results in the variation of the BSM spectrum with the cutoff scale, as can be seen in fig. 6. Since no BSM particles have been found in experiments hitherto, it is not useful to try to obtain a complete line of constant physics for the 2HDM by also keeping the masses of the BSM states fixed. Instead, it is more interesting to change the BSM couplings and investigate bounds on the additional scalar masses that are compatible with the SM conditions. For this purpose, we perform a scan in the hopping parameter (κ_1) for the BSM Higgs doublet. In sec. III D, we give details of this aspect of our work. Our strategy is to vary κ_1 within the (H_2) sector, while keeping all the other couplings fixed to their values used to tune the LPCP. It is found that the model still stays on the LPCP in this procedure. This can be understood by the nature of the weak quartic couplings. The most important conclusion of this scanning is that the BSM scalar states can be as light as about $0.15m_W$, and almost as heavy as the cutoff scale. Notice also that from experimental searches, the existence of BSM scalar particles with very low masses is not ruled out. There are recent works in this direction [70–72] and proposals to improve the studies at energies below 100 GeV. In [72] the range $25-70$ GeV is probed for the pseudoscalar m_A by looking for $\tau^-\tau^+$ resonances, while in [71] the search focuses on the diphoton final states around the range $70-110$ GeV.

We also study the finite temperature phase transition in this work, by performing simulations at different temporal extents with all the other parameters fixed to their values on the LPCP. From the analysis detailed in sec. III E, it is concluded that the custodial 2HDM with our choice of weak quartic couplings does not provide a first-order EWPT. Instead, through carrying out finite-size scaling for the susceptibility of the order parameter, it can be shown that the finite-temperature transition in (H_2) sector of the theory is a crossover that occurs at around the temperature $T \sim 2m_W$. This is similar to the scenario of the SM, and is in contrast with the prediction for a first-order phase transition from the perturbative investigation in [31].

The above findings for the bounds on the BSM masses, as well as the finite-temperature crossover behaviour, are from simulations performed at weak quartic couplings. Working in this weak-coupling regime can make our task simpler. This is because the interaction between the SM and the BSM sectors is small, such that the LPCP becomes largely insensitive to the change of some bare parameters (such as κ_1 and η_1 in eq. (10)) that numerically only affect the BSM sector. It is a suitable choice for the first step in our research programme, from which we have gained a significant amount of experience in tuning and calibrating the lattice computations, and have found interesting features of the custodial 2HDM. While this is an advantage from the practical perspective, there is no fundamental reason for the choice of small renormalized quartic couplings, and a complete investigation is necessary. In fact, many perturbative studies suggest that $\mathcal{O}(1)$ quartic couplings are required for a strong first-order EWPT. For instance, tree-level results [30, 31] indicate the need of large mass splitting amongst the BSM scalar states for the occurrence of this first-order transition. This condition is directly related to an enhanced value of the inter-flavour Higgs quartic coupling, namely,

η_3. Our future work will extend this exploration to the case of strong *renormalized* quartic couplings, in particular η_3. The tuning for a LPCP is expected to be much more challenging in this regime due to the renormalization effects of these couplings. In fact, given that the model is expected to be trivial, it is not even obvious whether a LPCP can be realized at large enough cutoff scales when some of the renormalized quartic couplings are large. To keep the value of a renormalized quartic coupling fixed at $\mathcal{O}(1)$, non-perturbative implementation of a suitable renormalization scheme is required. For this purpose, the use of the gradient flow on the scalar fields [73], similar to that on the gauge fields for the definition of g^2_{GF}, will be useful. Moreover, such a scheme is a prerequisite to investigate the issue of triviality in gauged scalar theories. To keep the value of a renormalized quartic coupling fixed at $\mathcal{O}(1)$, non-perturbative implementation of a suitable renormalization scheme is required. For this purpose, the use of the gradient flow on the scalar fields [73], similar to that on the gauge fields for the definition of g^2_{GF}, will be useful. Moreover, such a scheme is a prerequisite to investigate the issue of triviality in gauged scalar theories.

ACKNOWLEDGMENTS

GC and AR would like to acknowledge financial support from the Generalitat Valenciana (GENT program CIDEGENT/2019/040), Ministerio de Ciencia e Innovacion (PID2020-113644GB-I00). GC, AH, WSH, CJDL, AR and MS have received support from the CSIC-NSTC exchange grant 112-2927-I-A49-508. CJDL's work is partially supported by the NSTC project 112-2112-M-A49-021-MY3. Support from the NSTC project 112-2639-M-002-006-ASP is aknowledged by AH, WSH, CJDL and MS. This work also received funding from the European Union's Horizon Europe Framework Programme (HORIZON) under the ERA Chair scheme with grant agreement no.101087126 and the Ministry of Science, Research and Culture of the State of Brandenburg within the Centre for Quantum Technologies and Applications (CQTA). The authors thank ASGC (Academia Sinica Grid Computing Center, AS-CFII-114-A11, NSTC(NSTC 113-2740M-001-007) for provision of computational resources. Numerical computations for this work were also carried out on the HPC facilities at National Taiwan University and National Yang Ming Chiao Tung University.

Appendix A: Hybrid Monte-Carlo simulation for two-Higgs doublet models

We use the HMC algorithm in our simulations. This algorithm introduces a fictitious (simulation) time t on which all fields depend. The dynamics in the fictitious time is dictated by the Hamilton's equations of the following Hamiltonian

$$H(\Phi, U; \pi, p) = \frac{1}{2}\sum_{n,\alpha}(\pi_n^\alpha)^2 + \frac{1}{2}\sum_{\mu,a}\mathrm{Tr}\left(p_\mu^2\right) + S_{\mathrm{2HDM}}\,, \tag{A1}$$

where $p_\mu = p_\mu^a(x)\sigma_a,\ p_\mu^a \in \mathbb{R}$ are the algebra-valued momentum fields associated with the gauge fields and π_n^α are the real momenta conjugate to the real fields φ_n^α. The evolution of the fields is governed by

$$\begin{aligned} \dot{\pi}_n^\alpha(x,t) &= -\frac{\delta H}{\delta\varphi_n^\alpha(x,t)}\,, & \dot{p}_\mu^a(x,t) &= -\partial_{x,\mu}^a H\,, \\ \dot{\varphi}_n^\alpha(x,t) &= \frac{\delta H}{\delta\pi_n^\alpha(x,t)} = \pi_n^\alpha(x,t)\,, & \dot{A}_\mu^a(x,t) &= \frac{\delta H}{\delta p_\mu^a(x,t)}\,, \end{aligned} \tag{A2}$$

where $\partial_{x,\mu}^a$ is the algebra-valued differential operator defined in appendix A of [56], and A_μ^a the algebra-valued gauge fields, $U_\mu = \exp(-iA_\mu)$. The time evolution of U_μ can be written as

$$\dot{U}_\mu(x,t) = -ip_\mu(x,t)U_\mu(x,t),\ \text{(no sum in } \mu)\,, \tag{A3}$$

while numerically the evolution of the group-valued gauge fields is implemented by

$$U_\mu(x, t+\delta t) = \mathrm{e}\{-ip_\mu(x,t)\delta t\}U_\mu(x,t)\,. \tag{A4}$$

The corresponding momentum variables satisfy

$$\begin{aligned} i\dot{p}^a_\mu(x,t) = &-2\sum_n k_n \,\mathrm{Tr}\left[\hat{\Phi}^\dagger_n(x)\sigma_a U_\mu(x)\hat{\Phi}_n(x+\hat{\mu})\right] \\ &-2\beta\sum_\nu \mathrm{Tr}\left[\sigma_a\left(U_{\mu\nu}(x)-U^\dagger_{\mu\nu}(x)\right)-\sigma_a\left(U_{\mu\nu}(x-\hat{\nu})-U^\dagger_{\mu\nu}(x-\hat{\nu})\right)\right]. \end{aligned}$$

Finally, the equation of motion for the scalar momenta in the quaternion form are

$$\begin{aligned} -\dot{\pi}_1(y,t) = &-k_1\sum_\mu\{U_\mu(y)\Phi_1(y+\hat{\mu})+\Phi_1(y-\hat{\mu})U_\mu(y-\hat{\mu})\} \\ &+\Phi_1+4\eta_1\left[\mathrm{Tr}\left(\hat{\Phi}^\dagger_1\hat{\Phi}_1\right)-1\right]\Phi_1+2\mu^2\Phi_2+2\eta_3\,\mathrm{Tr}\left(\hat{\Phi}^\dagger_2\hat{\Phi}_2\right)\Phi_1 \\ &+2\eta_4\left[\mathrm{Tr}\left(\hat{\Phi}^\dagger_1\hat{\Phi}_2\right)\Phi_2+\mathrm{Tr}\left(\hat{\Phi}^\dagger_1\hat{\Phi}_2 i\sigma_3\right)\Phi_2 i\sigma_3\right] \\ &+2\eta_5\left[\mathrm{Tr}\left(\hat{\Phi}^\dagger_1\hat{\Phi}_2\right)\Phi_2-\mathrm{Tr}\left(\hat{\Phi}^\dagger_1\hat{\Phi}_2 i\sigma_3\right)\Phi_2 i\sigma_3\right] \\ &+2\left[\eta_6\,\mathrm{Tr}\left(\hat{\Phi}^\dagger_1\hat{\Phi}_1\right)+\eta_7\,\mathrm{Tr}\left(\hat{\Phi}^\dagger_2\hat{\Phi}_2\right)\right]\Phi_2+4\eta_6\,\mathrm{Tr}\left(\hat{\Phi}^\dagger_1\hat{\Phi}_2\right)\Phi_1\,, \end{aligned} \tag{A5}$$

$$\begin{aligned} -\dot{\pi}_2(y,t) = &-k_2\sum_\mu\{U_\mu(y)\Phi_2(y+\hat{\mu})+\Phi_2(y-\hat{\mu})U_\mu(y-\hat{\mu})\} \\ &+\Phi_2+4\eta_2\left[\mathrm{Tr}\left(\hat{\Phi}^\dagger_2\hat{\Phi}_2\right)-1\right]\Phi_2+2\mu^2\Phi_1+2\eta_3\,\mathrm{Tr}\left(\hat{\Phi}^\dagger_1\hat{\Phi}_1\right)\Phi_2 \\ &+2\eta_4\left[\mathrm{Tr}\left(\hat{\Phi}^\dagger_1\hat{\Phi}_2\right)\Phi_1-\mathrm{Tr}\left(\hat{\Phi}^\dagger_1\hat{\Phi}_2 i\sigma_3\right)\Phi_1 i\sigma_3\right] \\ &+2\eta_5\left[\mathrm{Tr}\left(\hat{\Phi}^\dagger_1\hat{\Phi}_2\right)\Phi_1+\mathrm{Tr}\left(\hat{\Phi}^\dagger_1\hat{\Phi}_2 i\sigma_3\right)\Phi_1 i\sigma_3\right] \\ &+2\left[\eta_6\,\mathrm{Tr}\left(\hat{\Phi}^\dagger_1\hat{\Phi}_1\right)+\eta_7\,\mathrm{Tr}\left(\hat{\Phi}^\dagger_2\hat{\Phi}_1\right)\right]\Phi_2+4\eta_7\,\mathrm{Tr}\left(\hat{\Phi}^\dagger_1\hat{\Phi}_2\right)\Phi_2\,. \end{aligned} \tag{A6}$$

The numerical implementation of multi-Higgs theories for GPU is available in [46]. Other than the HMC implementation, the code contains the computation of scalar observables, multi-Higgs and vector interpolators, smearing of gauge and scalar fields, as well as the gradient-flow tools such as the numerical solvers (including an adaptive step-size integrator) measurement functions for the action density, topological charge, etc.

[1] A. D. Sakharov, Soviet Physics Uspekhi **34**, 392 (1991), URL https://dx.doi.org/10.1070/PU1991v034n05ABEH002497.
[2] K. Kajantie, M. Laine, K. Rummukainen, and M. Shaposhnikov, Physical Review Letters **77**, 2887–2890 (1996), ISSN 1079-7114, URL http://dx.doi.org/10.1103/PhysRevLett.77.2887.
[3] H. G. Evertz, J. Jersak, and K. Kanaya, Nucl. Phys. B **285**, 229 (1987).
[4] K. Rummukainen, M. Tsypin, K. Kajantie, M. Laine, and M. Shaposhnikov, Nuclear Physics B **532**, 283–314 (1998), ISSN 0550-3213, URL http://dx.doi.org/10.1016/S0550-3213(98)00494-5.
[5] M. Laine, G. Nardini, and K. Rummukainen, Journal of Cosmology and Astroparticle Physics **2013**, 011–011 (2013), ISSN 1475-7516, URL http://dx.doi.org/10.1088/1475-7516/2013/01/011.
[6] M. D'Onofrio and K. Rummukainen, Physical Review D **93** (2016), ISSN 2470-0029, URL http://dx.doi.org/10.1103/PhysRevD.93.025003.
[7] R. L. Workman and Others (Particle Data Group), PTEP **2022**, 083C01 (2022).
[8] H. E. Haber and D. O'Neil, Physical Review D **83** (2011), ISSN 1550-2368, URL http://dx.doi.org/10.1103/PhysRevD.83.055017.
[9] D. O'Neil, Ph.D. thesis, UC, Santa Cruz, Phys. Dept. (2009), 0908.1363.
[10] H. E. Haber and D. O'Neil, Phys. Rev. D **74**, 015018 (2006), [Erratum: Phys.Rev.D 74, 059905 (2006)], hep-ph/0602242.
[11] E. Ma, Phys. Rev. D **73**, 077301 (2006), hep-ph/0601225.

[12] R. Barbieri, L. J. Hall, and V. S. Rychkov, Physical Review D **74** (2006), ISSN 1550-2368, URL http://dx.doi.org/10.1103/PhysRevD.74.015007.

[13] L. L. Honorez, E. Nezri, J. F. Oliver, and M. H. G. Tytgat, J. Cosmol. Astropart. Phys. **2007**, 028 (2007), ISSN 1475-7516, arXiv:hep-ph/0612275, URL http://arxiv.org/abs/hep-ph/0612275.

[14] M. Maniatis, A. von Manteuffel, O. Nachtmann, and F. Nagel, Eur. Phys. J. C **48**, 805 (2006), ISSN 1434-6044, 1434-6052, URL http://link.springer.com/10.1140/epjc/s10052-006-0016-6.

[15] I. P. Ivanov, M. Köpke, and M. Muhlleitner, Eur. Phys. J. C **78**, 413 (2018), ISSN 1434-6044, 1434-6052, arXiv:1802.07976 [hep-ph, physics:hep-th], URL http://arxiv.org/abs/1802.07976.

[16] I. P. Ivanov, Phys. Rev. D **75**, 035001 (2007), URL https://link.aps.org/doi/10.1103/PhysRevD.75.035001.

[17] A. Pilaftsis, Phys. Lett. B **706**, 465 (2012), 1109.3787.

[18] B. Grzadkowski, O. M. Ogreid, and P. Osland, JHEP **11**, 084 (2014), 1409.7265.

[19] J. a. M. Alves, F. J. Botella, G. C. Branco, F. Cornet-Gomez, M. Nebot, and J. a. P. Silva, Eur. Phys. J. C **78**, 630 (2018), 1803.11199.

[20] I. P. Ivanov, Phys. Rev. D **77**, 015017 (2008), URL https://link.aps.org/doi/10.1103/PhysRevD.77.015017.

[21] P. M. Ferreira, B. Grzadkowski, O. M. Ogreid, and P. Osland, J. High Energ. Phys. **2021**, 196 (2021), ISSN 1029-8479, URL https://link.springer.com/10.1007/JHEP02(2021)196.

[22] S. L. Glashow and S. Weinberg, Phys. Rev. D **15**, 1958 (1977).

[23] E. A. Paschos, Phys. Rev. D **15**, 1966 (1977).

[24] W.-S. Hou, Physics Letters B **296**, 179 (1992), ISSN 0370-2693, URL https://www.sciencedirect.com/science/article/pii/037026939290823M.

[25] W.-S. Hou and M. Kikuchi, Europhysics Letters **123**, 11001 (2018).

[26] L. Fromme, S. J. Huber, and M. Seniuch, JHEP **11**, 038 (2006), hep-ph/0605242.

[27] G. Branco, P. Ferreira, L. Lavoura, M. Rebelo, M. Sher, and J. P. Silva, Physics Reports **516**, 1 (2012), ISSN 03701573.

[28] M. Sher, Phys. Rept. **179**, 273 (1989).

[29] G. C. Dorsch, S. J. Huber, and J. M. No, J. High Energ. Phys. **2013**, 29 (2013), ISSN 1029-8479, arXiv:1305.6610 [astro-ph, physics:hep-ph], URL http://arxiv.org/abs/1305.6610.

[30] P. Basler, M. Krause, M. Muhlleitner, J. Wittbrodt, and A. Wlotzka, J. High Energ. Phys. **2017**, 121 (2017), ISSN 1029-8479, arXiv:1612.04086 [hep-ph], URL http://arxiv.org/abs/1612.04086.

[31] J. Bernon, L. Bian, and Y. Jiang, J. High Energ. Phys. **2018**, 151 (2018), ISSN 1029-8479, arXiv:1712.08430 [hep-ph], URL http://arxiv.org/abs/1712.08430.

[32] K. Kainulainen, V. Keus, L. Niemi, K. Rummukainen, T. V. I. Tenkanen, and V. Vaskonen, JHEP **06**, 075 (2019), 1904.01329.

[33] M. Luscher and P. Weisz, Nucl. Phys. B **290**, 25 (1987).

[34] M. Luscher and P. Weisz, Nucl. Phys. B **295**, 65 (1988).

[35] M. Luscher and P. Weisz, Nucl. Phys. B **318**, 705 (1989).

[36] M. Luscher and P. Weisz, Phys. Lett. B **212**, 472 (1988).

[37] M. Aizenman and H. Duminil-Copin, Annals Math. **194**, 163 (2021), 1912.07973.

[38] M. Wurtz, R. Lewis, and T. G. Steele, Phys. Rev. D **79**, 074501 (2009), ISSN 1550-7998, 1550-2368.

[39] R. Lewis and R. M. Woloshyn, Phys. Rev. D **82**, 034513 (2010), ISSN 1550-7998, 1550-2368, arXiv:1005.5420 [hep-lat, physics:hep-ph].

[40] A. Maas, Nucl. Part. Phys. Proc. **273-275**, 1604 (2016), 1410.2740.

[41] L. Niemi, M. J. Ramsey-Musolf, and G. Xia (2024), 2405.01191.

[42] M. Laine and K. Rummukainen, Nucl. Phys. B **597**, 23 (2001), hep-lat/0009025.

[43] G. Catumba, A. Hiraguchi, K. Jansen, Y.-J. Kao, A. Ramos, M. Sarkar, G. W. S. Hou, and C. J. D. Lin, PoS **LATTICE2024**, 145 (2025), 2412.13896.

[44] G. Catumba, A. Hiraguchi, G. W. S. Hou, K. Jansen, Y.-J. Kao, C. J. D. Lin, A. Ramos, and M. Sarkar, PoS **LATTICE2023**, 087 (2024), 2312.04178.

[45] M. Sarkar, G. Catumba, A. Hiraguchi, G. W. S. Hou, K. Jansen, Y.-J. Kao, C. J. D. Lin, and A. Ramos Martinez, PoS **LATTICE2022**, 388 (2023), 2210.09855.

[46] G. Catumba, URL https://igit.ific.uv.es/gtelo/latticegpu.jl/-/tree/su2-higgs.

[47] A. Ramos, *Latticegpu.jl: A framework for lattice computations on the gpu*, URL https://ific.uv.es/~alramos/docs/LatticeGPU.

[48] U. Wolff (ALPHA), Comput. Phys. Commun. **156**, 143 (2004), [Erratum: Comput.Phys.Commun. 176, 383 (2007)], hep-lat/0306017.

[49] A. Ramos, *Aderrors.jl,*, URL https://igit.ific.uv.es/alramos/aderrors.jl.

[50] A. Ramos, Comput. Phys. Commun. **238**, 19 (2019), 1809.01289.

[51] N. G. Deshpande and E. Ma, Phys. Rev. D **18**, 2574 (1978), URL https://link.aps.org/doi/10.1103/PhysRevD.18.2574.

[52] J. Frohlich, G. Morchio, and F. Strocchi, Phys. Lett. B **97**, 249 (1980), print-80-0557 (SNS,PISA).

[53] J. Frohlich, G. Morchio, and F. Strocchi, Nucl. Phys. B **190**, 553 (1981).

[54] W. Bock, H. G. Evertz, J. Jersák, D. P. Landau, T. Neuhaus, and J. L. Xu, Phys. Rev. D **41**, 2573 (1990), URL https://link.aps.org/doi/10.1103/PhysRevD.41.2573.

[55] Z. Fodor, J. Hein, K. Jansen, A. Jaster, and I. Montvay, *Simulating the Electroweak Phase Transition in the SU(2) Higgs*

Model (1994), arXiv:hep-lat/9409017, URL http://arxiv.org/abs/hep-lat/9409017.
[56] M. Lüscher, JHEP **08**, 071 (2010), [Erratum: JHEP 03, 092 (2014)], 1006.4518.
[57] A. Ramos, *The Yang-Mills gradient flow and renormalization* (2015), number: arXiv:1506.00118 arXiv:1506.00118 [hep-lat], URL http://arxiv.org/abs/1506.00118.
[58] M. Lüscher and P. Weisz, J. High Energ. Phys. **2011**, 51 (2011), ISSN 1029-8479, arXiv:1101.0963 [hep-lat, physics:hep-th].
[59] A. Maas and L. Pedro, Phys. Rev. D **93**, 056005 (2016).
[60] M. B. Wurtz, Ph.D. thesis, York U., Canada, York U., Canada (2015).
[61] M. Wurtz and R. Lewis, Phys. Rev. D **88**, 054510 (2013), URL https://link.aps.org/doi/10.1103/PhysRevD.88.054510.
[62] M. Peardon, J. Bulava, J. Foley, C. Morningstar, J. Dudek, R. G. Edwards, B. Joó, H.-W. Lin, D. G. Richards, and K. J. Juge (Hadron Spectrum Collaboration), Phys. Rev. D **80**, 054506 (2009).
[63] G. Catumba, Ph.D. thesis, U. Valencia (main) (2025), URL https://hdl.handle.net/10550/105754.
[64] I. Montvay and G. Münster, *Quantum Fields on a Lattice*, Cambridge Monographs on Mathematical Physics (Cambridge University Press, 1994).
[65] W. Langguth, I. Montvay, and P. Weisz, Nuclear Physics B **277**, 11 (1986), ISSN 05503213, URL https://linkinghub.elsevier.com/retrieve/pii/055032138690430X.
[66] F. Csikor, Z. Fodor, P. Hegedus, and A. Piroth, Phys. Rev. D **60**, 114511 (1999), hep-ph/9906260.
[67] A. Hasenfratz, K. Jansen, J. Jersak, C. B. Lang, H. Leutwyler, and T. Neuhaus, Z. Phys. C **46**, 257 (1990).
[68] M. D'Onofrio, K. Rummukainen, and A. Tranberg, Phys. Rev. Lett. **113**, 141602 (2014), 1404.3565.
[69] G. C. Dorsch, S. J. Huber, K. Mimasu, and J. M. No, Phys. Rev. Lett. **113**, 211802 (2014), 1405.5537.
[70] A. M. Sirunyan et al. (CMS), JHEP **05**, 210 (2019), 1903.10228.
[71] G. Aad et al. (ATLAS), JHEP **01**, 053 (2025), 2407.07546.
[72] A. Hayrapetyan et al. (CMS), Phys. Lett. B **860**, 139067 (2025), 2405.18149.
[73] C. Monahan and K. Orginos, Phys. Rev. D **91**, 074513 (2015), 1501.05348.